UPPSALA UNIVERSITET

Examensarbete vid Institutionen för geovetenskaper
Degree Project at the Department of Earth Sciences
ISSN 1650-6553 Nr 568

Modelling the Effects of Climate Change on Future DOC Export to Lake Mälaren Using a Generalized Watershed Loading Functions (GWLF) Model

Modellering av effekterna från klimatförändringar på framtida löst organiskt kol (DOC) export till Mälaren med hjälp av en GWLF-modell

Klara Lindqvist

INSTITUTIONEN FÖR GEOVETENSKAPER
DEPARTMENT OF EARTH SCIENCES

Examensarbete vid Institutionen för geovetenskaper
Degree Project at the Department of Earth Sciences
ISSN 1650-6553 Nr 568

Modelling the Effects of Climate Change on Future DOC Export to Lake Mälaren Using a Generalized Watershed Loading Functions (GWLF) Model

Modellering av effekterna från klimatförändringar på framtida löst organiskt kol (DOC) export till Mälaren med hjälp av en GWLF-modell

Klara Lindqvist

ISSN 1650-6553

Published at Department of Earth Sciences, Uppsala University (www.geo.uu.se), Uppsala, 2022

Abstract

Modelling the Effects of Climate Change on Future DOC Export to Lake Mälaren Using a Generalized Watershed Loading Functions (GWLF) Model
Klara Lindqvist

Browning of boreal freshwaters due to an increased export of terrestrial dissolved organic carbon (DOC) has been observed for some decennia. Drivers include recovery from acid deposition and changing climate and land cover. Lake Mälaren provides the Swedish capital Stockholm with drinking water and an increased future browning of the lake could demand more treatment to produce acceptable drinking water. Knowledge of what can be expected in a changing climate is therefore needed. The aim of this study was to evaluate; (1) The performance of the GWLF model simulations of hydrology and DOC export for 13 catchments draining into the Galten and Ekoln basins in lake Mälaren; (2) How simulated DOC export from the 13 catchments would change in response to climate scenarios RCP2.6, 6.0 and 8.5; and (3) If climate change impact on DOC export to lake Mälaren potentially will demand more treatment of the lake water in the future to produce acceptable drinking water to the Stockholm area. All data used were open access and include temperature, precipitation, discharge, total organic carbon (TOC) and water colour, land cover and soil types. In comparison to other studies, good model performance was found when simulating daily streamflow, baseflow, surface runoff, daily DOC loads and monthly DOC loads. Model simulations of DOC concentrations were less certain, but for some catchments similar results were obtained as in other studies. Increased air temperature resulted in higher simulated soil temperatures and a longer growing season. An increase in both annual precipitation and evapotranspiration resulted in only slight increase in simulated annual streamflow. There were, however, large seasonal impacts on streamflow with higher winter flows and lower spring flood. Annual DOC loads increased, mainly due to increased DOC concentrations over the whole year, as the annual streamflow did not change greatly. Increased winter streamflow and DOC concentrations resulted in large increases in DOC loads. The impact was larger for the higher emission scenarios. DOC loading to Galten and Ekoln increased in all future scenarios during winter, with a likely impact on DOC concentrations in the eastern basins as well. Increased loads to Ekoln are likely to impact the drinking water production of Stockholm more direct than the increases in Galten, as the Ekoln water has a shorter transit time to the drinking water withdrawals. The GWLF model shows much promise in predicting DOC concentrations and loads to lake Mälaren in a changing climate. To estimate the effects of DOC export to lake Mälaren on future drinking water production, further work also needs to be done on in-lake transport and processes.

Keywords: Hydrology, DOC, browning, climate change, drinking water production, Mälaren

Degree Project E1 in Earth Science, 1GV025, 30 credits
Supervisors: Don Pierson and Stephan Köhler
Department of Earth Sciences, Uppsala University, Villavägen 16, SE-752 36 Uppsala (www.geo.uu.se)

ISSN 1650-6553, Examensarbete vid Institutionen för geovetenskaper, No. 568, 2022

The whole document is available at www.diva-portal.org

Populärvetenskaplig sammanfattning

Modellering av effekterna från klimatförändringar på framtida löst organiskt kol (DOC) export till Mälaren med hjälp av en GWLF-modell

Klara Lindqvist

Sjöar och vattendrag på nordliga breddgrader har under flera decennier blivit allt brunare. Orsaken är att löst organiskt kol, Dissolved Organic Carbon (DOC), som bland annat utgörs av humusämnen, transporteras till ytvatten från omkringliggande mark. De vanligaste förklaringarna till detta är en återhämtning från tidigare försurning orsakad av sulfatdeposition, klimatförändringar och en ändrad markanvändning. Mälaren är den primära dricksvattenkällan för Stockholm och om vattnet fortsätter bli brunare kan det innebära att reningsprocessen behöver ändras för att undvika produktion av hälsofarliga biprodukter i dricksvattnet. Det är därför viktigt att ta reda på hur ett ändrat klimat kan påverka export av DOC till Mälaren. Målet med den här studien var att undersöka tre frågor kopplade till framtida DOC i Mälaren. Den första var hur väl GWLF-modellen kunde användas på 13 avrinningsområden i Mälaren. Modellen simulerar vattnets väg från nederbörd till vattendrag samt hur DOC bryts ned och transporteras ut från marken. Den andra frågan var hur simulerad nedbrytning och export av DOC skulle påverkas av tre olika klimatscenarion, Representative Concentration Pathways (RCP), som baseras på tre olika nivåer av utsläpp av växthusgaser. Dessa var RCP2.6, 6.0 och 8.5, där högre nivåer av utsläpp av växthusgaser är kopplade till en högre siffra. Den tredje och sista frågan var att utvärdera om klimatförändringar kommer påverka hur mycket DOC som når Mälaren och ifall detta kan väntas påverka framtida dricksvattenproduktion i området. All data som har använts för att genomföra studien har varit så kallad "Öppna data", som är fritt för alla att ladda ned, från både svenska, europeiska och andra internationella databaser. Data som använts är temperatur, nederbörd, vattenflöde, vattenkemi, vegetationstäcke och jordarter.

Modellen visade ett tillfredsställande resultat i att simulera dagligt vattenflöde och både daglig och månatlig DOC-export. Den var mer osäker på att simulera koncentrationerna av DOC, men i flera områden lyckades den prestera liknande som i många andra studier. Alla framtida klimatscenarier visade en ökning av nederbörd, luft- och marktemperatur, avdunstning och antal växtdagar. Det syntes en större påverkan vid högre utsläppscenarion och effekterna ökade för RCP6.0 och 8.5 mot slutet av detta sekel. För RCP2.6 kunde en återhämtning ses mot slutet av seklet på grund av en minskning av utsläpp av växthusgaser. Den högre årsnederbörden resulterade inte i motsvarande ökning i årsvattenflöde på grund av att även avdunstningen ökade. Simuleringen visade en säsongsbunden effekt på DOC-export med en ökning under vintermånaderna men ingen skillnad under sommaren. Koncentrationer av DOC ökade däremot under hela året, dock mer under vintern. Årsexport av DOC från de undersökta avrinningsområdena till de två bassänger i Mälaren som mottar vattnet, Galten och Ekoln, ökade för alla framtida klimatscenarion. Ökningen var ett resultat av ökad vinterexport då det under sommarmånaderna antingen inte fanns någon skillnad eller en liten minskning av DOC-export. Detta påverkar sannolikt även de östra bassängerna där Stockholm tar sitt dricksvatten. Ökad DOC-export till Ekoln skulle troligen påverka Stockholms dricksvattenproduktion mer eftersom bassängerna har ett direkt vattenutbyte. GWLF-modellen som användes här visade potential i att simulera DOC-export till Mälaren i ett ändrat klimat. För att uppskatta framtida påverkan av DOC-export på dricksvattenproduktionen kring Mälaren behöver även processer som sker i sjön undersökas.

Nyckelord: Hydrologi, DOC, brunifiering, klimatförändringar, dricksvattenproduktion, Mälaren

Examensarbete E1 i geovetenskap, 1GV025, 30 hp
Handledare: Don Pierson och Stephan Köhler
Institutionen för geovetenskaper, Uppsala universitet, Villavägen 16, 752 36 Uppsala (www.geo.uu.se)

ISSN 1650-6553, Examensarbete vid Institutionen för geovetenskaper, Nr 568, 2022

Hela publikationen finns tillgänglig på www.diva-portal.org

Table of Contents

1 Introduction

Browning of boreal surface waters has been observed for some decennia (Monteith et al. 2007; de Wit et al. 2016). The browning is mainly a result of an increased export of dissolved organic carbon (DOC) from the terrestrial environment, but increased iron concentrations have also been shown to influence the colour (Kritzberg & Ekström 2012; Kritzberg et al. 2020). Different causes for the browning have been identified, such as an increased mobilization of organic matter in soils following a decreased sulphate deposition, changing climate and land cover (Kritzberg et al. 2020). Although correlation between browning and all three drivers have been shown, climate change and land cover can be expected to have the most impact for future browning, as the effects of recovery from sulphate deposition decreases with time.

Increased DOC in freshwaters can negatively impact aquatic ecology (Creed et al. 2018), contribute to CO_2 emissions (Lapierre et al. 2013) and complicate drinking water production (Richardson et al. 2007; Lavonen et al. 2013). The latter is important for lake Mälaren, the third largest lake in Sweden, that serves as drinking water source for over 2.2 million people (Norrvatten n.d.; Stockholm Vatten och Avfall n.d.). Therefore, knowledge of future changes of water quality in the lake is of great importance, and a continued browning of the water could impose challenges for drinking water production. As the organic content of the water increases, there is an increased need to remove colour, odour, and taste to keep producing acceptable drinking water to consumers. In addition, the increased organic material can react with disinfectants and create disinfectant by-products, some of which can be carcinogenic (Richardson et al. 2007).

A warmer climate is expected to increase the production and decomposition of terrestrial organic carbon due to higher soil temperatures and a prolonged growth season (Finstad et al. 2016). This will result in more available carbon that could be transported by water from soils. The impact of precipitation is uncertain, but an increased water flow through the soil column has the possibility to transport more carbon to freshwaters (Fork et al. 2020). A shift towards more rain instead of snow during winters would lead to higher winter streamflow. In most regions this would likely increase browning of freshwaters, with the exception of regions where precipitation and runoff are already high, where instead dilution could occur (de Wit et al. 2016).

1.1 Dissolved organic carbon (DOC)

Organic material, such as leaf litter, roots and accumulating peat moss contribute to the organic carbon pool in the boreal region. The organic matter accumulating on the forest floor is subjected to decomposition by microorganisms (Futter et al. 2007). Decomposition of organic matter is impacted by substrate quality, temperature, and moisture levels (Davidsson & Janssens 2006; Wickland & Neff 2007). More complex molecular structure of the substrate results in higher temperature sensitivity (Davidson & Janssens 2006). Water content of the soil determines if decomposition is aerobic or

anaerobic, the former often occurring at a higher rate. Due to the lower decomposition rates in anaerobic environments, such as wetlands, peatlands, and permafrost areas, these tend to accumulate carbon and work as carbon sinks. Very low moisture conditions can also limit decomposition (Wickland & Neff 2007).

Organic carbon can be present as either particulate organic carbon (POC) or dissolved organic carbon (DOC). Following decomposition, DOC can be transported by water through and out of the soil column. DOC is made up of different organic compounds that can pass through a filter of <0.45 µm (Temnerud 2005), such as humic substances, macromolecular hydrophilic acids, low-molecular-weight organics, carboxylic acids, and amino acids (Aitkenhead et al. 2003). Due to the yellow to brown colour of humic substances, light absorbance at different wavelengths, such as 420nm, can be used to assess the concentration of DOC in the water (Temnerud 2005).

Terrestrially derived DOC undergoes several processes once transported to streams and lakes, including mineralization, flocculation, and photolytic processing (von Wachenfeldt & Tranvik 2008; Köhler et al. 2013). These lead to reduced DOC concentrations and less brown water. Lake water colour has been shown to be stronger for lakes with shorter water retention time (Köhler et al. 2013) as well as a large catchment area compared to lake size (von Wachenfeldt & Tranvik 2008). Köhler et al. (2013) showed that as the water retention time increased, water colour was more impacted by DOC and less by colloidal associated iron. This was explained by a half-life of 1.7 and 0.6 years for water colour and colloidal associated iron respectively, whereas DOC had a half-life of 6.1 years. In addition to water retention time, pH also impacts water colour as it affects the interactions of iron and organic matter (Köhler et al. 2013).

In the case of Mälaren, water retention time increases from west to east and north to south due to the movement of the water (figure 3). The longest water retention time is found near the lake outlet located in the easternmost part of the lake where it is approximately 2.8 years (Wallin et al. 2000). The shorter lake water retention time in western and northern Mälaren, where the basins are only fed with water directly from the catchments, results in higher DOC concentrations. Despite the raw water used by the drinking water treatment plants having a higher retention time with a lower incoming DOC level, the molecular composition in this water may make removal at the water treatment plant difficult (Köhler et al. 2016). According to SMHI (Eklund et al. 2018) climate change will likely change the water retention time of Mälaren, with possibly shorter retention times, which would consequently affect the fate of DOC in the lake.

1.2 Hydrological and DOC modelling

Hydrological models are important tools for prediction of runoff and streamflow in response to climate change. In addition, hydrological models set up the basis for water quality modelling, i.e. simulations of nutrient transport and fluxes (e.g. DOC) from terrestrial environments. The hydrological GWLF (Generalized Watershed Loading Functions) model is a lumped-parameter model, first developed in

1987 by Haith and Shoemaker (Haith & Shoemaker 1987; Haith et al. 1996). It was later coupled with a DOC model in the CLIME (Climate and Lake Impacts in Europe) project which was used to assess the impact of climate change on lake DOC in the UK, Ireland, Finland and Sweden (Naden et al. 2009; Schneiderman et al. 2009).

The GWLF model has successfully modelled catchment runoff in numerous studies in different countries, including Finland (Einola 2013), Ireland (Jennings et al. 2009), Sweden (Moore et al. 2008), USA (Moore 2007; Niraula et al. 2013) and China (Qi et al. 2017). The main objectives in these studies were to simulate sediment yield and nutrient loads to lakes.

1.3 Study aim

The aim of this study was to examine how future climate will affect the production and export of DOC to lake Mälaren. The main objective was to assess whether DOC is likely to increase in the future in the Görväln basin and subsequently affect the raw water used by the drinking water treatment plant Norrvatten. The model chosen to answer these questions was the GWLF-Hydrology-DOC model. As this DOC model was originally developed for peat soils and previously only has been applied on a limited number of catchments, another interest was to evaluate the performance of this model on a range of different catchments, mainly dominated by coniferous forest. The study questions that were asked are:

1) How well can the coupled GWLF-Hydrology-DOC model simulate streamflow and DOC export from 13 different study catchments in lake Mälaren?

2) How will the simulated DOC from the GWLF-Hydrology-DOC model respond to climate change scenarios, based on RCP2.6, 6.0 and 8.5, in the 13 catchments?

3) Will climate change impact on DOC export to lake Mälaren potentially demand more treatment of the lake water in the future to produce acceptable drinking water to the Stockholm area?

2 Methods

2.1 Generalized Watershed Loading Functions (GWLF)

The GWLF model can be run in different software. In this study, the Vensim (Ventana Systems Inc.) software was used. The basis of this version of GWLF was first developed by the New York City Department of Environmental Protection (NYC DEP) (Schneiderman et al. 2002; Jennings et al. 2009). The GWLF-Hydrology-DOC model used here was developed during the CLIME project, with only slight modifications done after. The two different components, hydrology and DOC, are described further below.

2.1.1 GWLF-Hydrology

The GWLF-Hydrology model used here is in large the same that is described by Schneiderman et al. (2009). The model simulates water balance on a daily time step, driven by catchment averaged daily air temperature and precipitation. Water is added to the model through precipitation and exits through either evapotranspiration or discharge. To preserve the long-term water balance, a catchment specific *precipitation correction factor* is used. Assuming that these are the only fluxes of water in to and out of the system, the precipitation used to drive the model is modified accordingly. Snow accumulates during below-zero temperatures and starts to melt when temperatures rise over zero, regulated by the catchment specific *melt coefficient*.

Precipitation and snowmelt will then either produce surface runoff or infiltrate into the soil. Runoff is governed by the Soil Conservation Service (SCS) Curve number equation (Haith et al. 1996). Curve numbers (CN) are assigned to each land use and the CN's used in this study were developed by Moore (2008) based on land cover and soil types. The CORINE land use classification was used. They are adjusted depending on the 5-day antecedent moisture conditions that are based on precipitation and whether the time is during a dormant or growing season. Growing season is active when the mean daily temperature is 5°C for 5 days in a row and the dormant season is when the mean daily temperature has been below 5°C for 5 days in a row. Additionally, a 10-day delay was used to avoid rapid changes in the seasonal status, so that when shifting from one season to another the temperature threshold must be exceeded for 10 days or more. A *CN-adjustment factor* adjusts the CN's for pervious land covers to increase or decrease runoff. Runoff is divided into delayed and direct runoff. Delayed runoff is stored in the river channel and connecting lakes and subjected to evaporation before it is released to the streamflow as a fraction of the channel storage, determined by the *channel flow coefficient*. When the channel storage exceeds maximum, all stored water above this limit is released directly. Direct runoff is a fraction of the total runoff, that immediately influences streamflow determined by the *channel flow coefficient*.

The water that is not directed to the runoff component of streamflow is infiltrated into an unsaturated zone. From this, water can either be lost through evapotranspiration (ET) or percolate to the saturated

zone once the soil exceeds its *soil water capacity*. Potential evapotranspiration (PET) is calculated with the Hamon-method (Hamon, 1961), using an approximation of the saturated vapor pressure developed by Bosen (1960). Actual evapotranspiration (AET) is then determined by PET and the seasonal cover coefficient as well as an *ET restriction coefficient* that restricts ET when soil moisture reaches the wilting point. The restriction coefficient was calculated as a weighted average for each catchment based on water stress coefficients (K_s) for different land covers developed by the FAO (Allen et al. 1998). Each land cover is assigned an Evapotranspiration Cover Coefficient for both dormant and growing season. A simple approach was used where land covers were assigned a cover coefficient of either 0.3 or 1.0 with leafy land cover given a cover coefficient of 0.3 during dormant season and 1.0 during growing season. Perennial crops and coniferous forest were given a cover coefficient of 1.0 year-round.

Soil water capacity reflects the field capacity of the unsaturated zone and water percolates to the saturated zone when this is exceeded. From the saturated zone, the water can take two paths. It can either leave the soil storage as baseflow or it can further percolate to the deep saturated zone. A fraction of the water in the saturated zone contributes to the streamflow as baseflow, and this is determined by the *recession coefficient*. As long as there is water in the saturated zone it also enters the deep saturated zone until the *deep soil water capacity* of the deep saturated zone is exceeded. Water leaves the deep saturated zone and contributes to streamflow as slow baseflow, which is a fraction of the water in the deep saturated zone and regulated by the *slow recession coefficient*.

Finally, direct runoff, stored runoff, baseflow and slow baseflow are added together to calculate the total streamflow which can be converted from GWLF's depth-based calculation (cm day^{-1}) to discharge in m^3 s^{-1} by multiplying with catchment area and adjusting the time. All catchment specific parameters are written in italics above as well as in figure 1 and are summarized in table 1. These parameters are represented by one single value averaged over the whole catchment. All catchment specific parameters except for the ET restriction coefficient were calibrated.

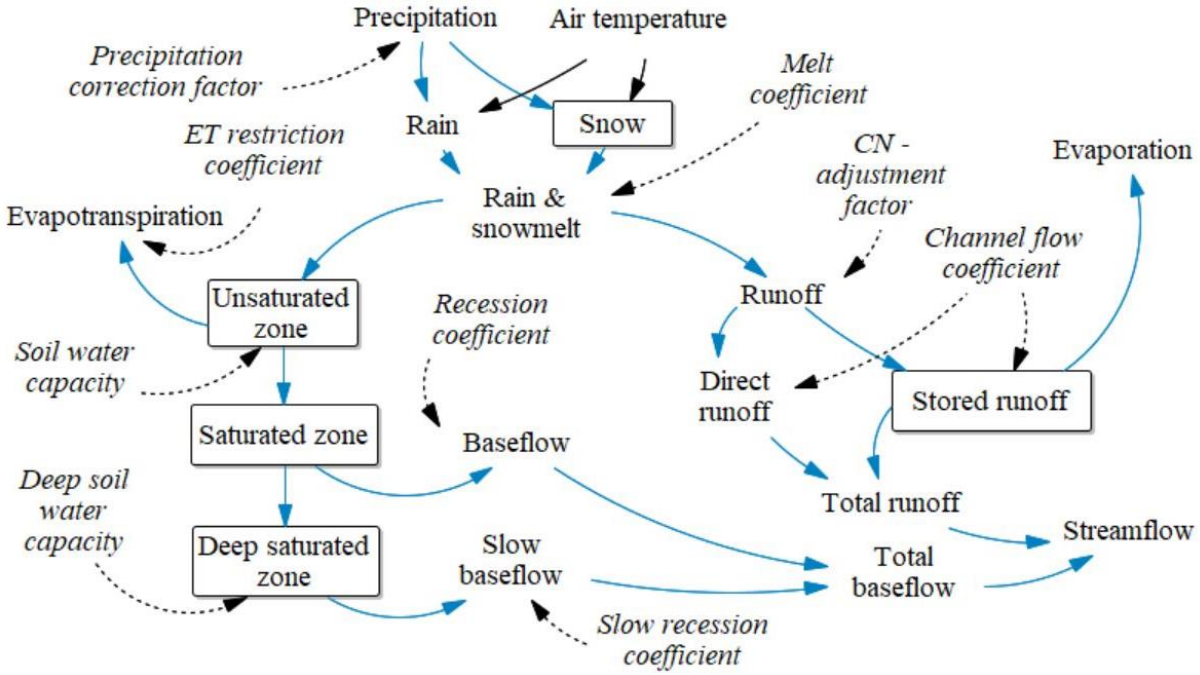

Figure 1 Overview of the hydrology model. Precipitation and air temperature are driving the model, and streamflow is the final output. Blue arrows indicate the pathways of water and its direction between different hydrological components. Dashed arrows and parameters in italics are catchments specific parameters, either calculated or calibrated. Boxed parameters indicate storage and other parameters in normal font indicate fluxes of water.

Table 1 Hydrological catchment specific parameters where every parameter represents an average over the whole catchment, shown in italics in figure 1. All parameters were calibrated, except for the ET restriction coefficient which was derived from literature.

Hydrological parameters	Explanation
Precipitation correction factor	Corrects precipitation to conserve the long-term water balance
Melt coefficient	Determines snowmelt as a function of air temperature (cm day^{-1} $°C^{-1}$)
CN-adjustment factor	Corrects CN of pervious land covers to increase or decrease runoff
Channel flow coefficient	Adjusts amount of runoff released to streamflow
ET restriction coefficient	Restricts ET when soil moisture is at wilting point, land cover specific
Soil water capacity	Field capacity of the unsaturated zone (cm)
Recession coefficient	Fraction of the saturated zone that will generate baseflow (day^{-1})
Deep soil water capacity	Determines how much water the deep saturated zone can hold (cm)
Slow recession coefficient	Fraction of the deep saturated zone that will generate slow baseflow (day^{-1})

2.1.2 GWLF-DOC

The GWLF-DOC model was first developed during the CLIME project and is described in detail in Naden et al. (2009). It was developed primarily to model DOC production and export in peat dominated catchments. As chemical processes such as sorption-desorption and mineralisation were assumed to be less important in peat soils, these are not represented in the model. As part of the study aim, the goal of this study was to examine how well this model can be applied on catchments dominated by coniferous forest, where these processes are known to occur. DOC export is assumed to be dominated by lateral transport and is a function of the available DOC store and water flow in the different hydrological paths described in the previous section (Naden et al. 2009). The decomposition processes leading to DOC

production is represented in a single carbon pool, as was done by Naden et al. (2009). The DOC-model contains six catchments specific parameters (figure 2; table 2).

Decomposition of organic material is impacted by temperature and soil moisture (Naden et al. 2009). To represent this in the model, production of DOC through decomposition of organic material is determined by an Arrhenius equation combined with a soil moisture dependent decomposition equation developed from experiments by Mitchell and McDonald (1992). The resulting equation that is used for DOC production in the model is

$$D_{T,S} = a_{T_{ref}} \left\{ exp\left(-b \left[\left(\frac{(S_{max} - S)}{1.6 S_{max}} - 0.35 \right)^2 - 0.1225 \right] \right) \right\} \times exp\left(\frac{E_a}{R} \left[\frac{1}{T_{ref}} - \frac{1}{T} \right] \right) \text{ (Eq. 1)}$$

where $D_{T,S}$ is DOC production rate (gC m^{-2} day^{-1}) at soil moisture S, represented by the left factor of equation 1 and soil temperature T (K), given by the right factor of equation 1. Soil moisture is given by a relationship between the soil water capacity, S_{max} (cm) and the soil water content S (cm) of the unsaturated zone. T_{ref} is the reference soil temperature, which in this study is set to 10°C (283 K). R is the universal gas constant (6.928×10^{-4} kJ K^{-1} gC^{-1}). Soil temperature is determined from a 10-day moving average of the air temperature above zero. The slower soil warming observed in spring is represented by an extended moving average over 30-days for two months after the snowpack has a depth of 2 cm (Naden et al. 2009). A comparison with measured and simulated soil temperatures from the SITES stations Asa and Svartberget, where soil temperatures are measured at a depth of 10 and 20 cm, shows a good correlation of this method with R^2=0.95 and 0.94 respectively.

The catchment specific parameters needed to run this equation is a_{Tref}, b and E_a, where a_{Tref} is the anaerobic DOC production rate (gC m^{-2} day^{-1}), b is the rate of change in DOC production dependent on soil moisture, also termed the aerobic decomposition rate and E_a is the activation energy (kJ gC^{-1}) (Naden et al. 2009). A higher activation energy leads to a higher temperature sensitivity (Davidson & Janssens 2006). From the soil moisture dependent factor in equation 1, decomposition will increase as the soil water decreases until it reaches a certain point, where decomposition will decrease as soil water continues to decrease. This is determined by the aerobic decomposition rate b in the equation. The calibration range for b was constrained based on a study by von Arnold et al. (2005) and the ratio found between aerobic and anaerobic decomposition. Activation energies for each catchment were derived from literature and based on Q_{10} values reported for different land covers for the reference temperature 10°C (Vanhala et al. 2008; Karhu et al. 2010; Klimek et al. 2020). Anaerobic DOC production rate and aerobic decomposition were calibrated.

Following decomposition, DOC will interact with the hydrological pathways previously described and be washed out from the soil storage. As no chemical processes are included in this simple model, all DOC produced by the model will be available for washout (Naden et al. 2009). DOC can be lost through three different hydrological pathways dependent on the current water balance of the system. These are runoff, percolation, and deep percolation, the two latter making up the baseflow. DOC loss will only occur from DOC producing land covers which were broad leaved, mixed and coniferous

forests, natural grasslands, transitional woodland shrub, inland marshes and peat bogs, based on the CORINE land cover classification.

DOC washout through runoff (W_{runoff}, gC m^{-2} day^{-1}) is defined for each land cover and is diluted during high rainfall or snowmelt events (Naden et al. 2009). This is given by

$$W_{runoff} = k_{fast} C \times \min\left(R_{luDOC}, R_0\right) \frac{S}{S_{max}} \quad \text{(Eq. 2)}$$

where k_{fast} is the fast rate of washout, given as a fraction cm^{-1}, C is the available DOC, R_{luDOC} is the runoff from DOC producing land covers, R_0 is the threshold that determines when dilution occurs, and the soil moisture dependence term adjusts for the control of pore space connectivity on DOC (Naden et al. 2009).

DOC washout through subsurface flow (W_{ssf}, gC m^{-2} day^{-1}) is given by

$$W_{ssf} = k_{slow} C \times P \quad \text{(Eq. 3)}$$

where k_{slow} is the slow rate of washout, given as a fraction cm^{-1}, C is the available DOC and P is percolation (cm day^{-1}).

In many forested catchments, the organic layer is underlain by a mineral soil. This will affect the slow subsurface washout as DOC concentrations in this layer will be different, and DOC may adsorb to mineral grains (Naden et al. 2009). To account for this, a *mineral adjustment factor*, *M* adjusts the washout of DOC from slow subsurface flow ($W_{slowssf}$, gC m^{-2} day^{-1}), given by

$$W_{slowssf} = k_{slow} C P_{deep} \left(\frac{M A_{min} + A_{peat}}{A_{luDOC}}\right) \quad \text{(Eq. 4)}$$

where C is the available DOC, P_{deep} is the deep percolation, A_{min} is the area of soils with a mineral soil horizon, A_{peat} is the area of deep peats and A_{luDOC} is the area of DOC producing land covers. Fast rate of washout (k_{fast}) in equation 2 is computed by multiplying the slow rate of washout (k_{slow}) with a *washout ratio coefficient*. The slow rate, k_{slow}, *washout ratio coefficient* and *mineral adjustment factor* are calibrated.

At each time step, the available DOC storage is updated based on production and loss, and the total washout is summed. Streamflow concentrations are calculated based on the total DOC loss and streamflow contributions from the entire catchment. Both DOC concentrations and DOC loads are given as output.

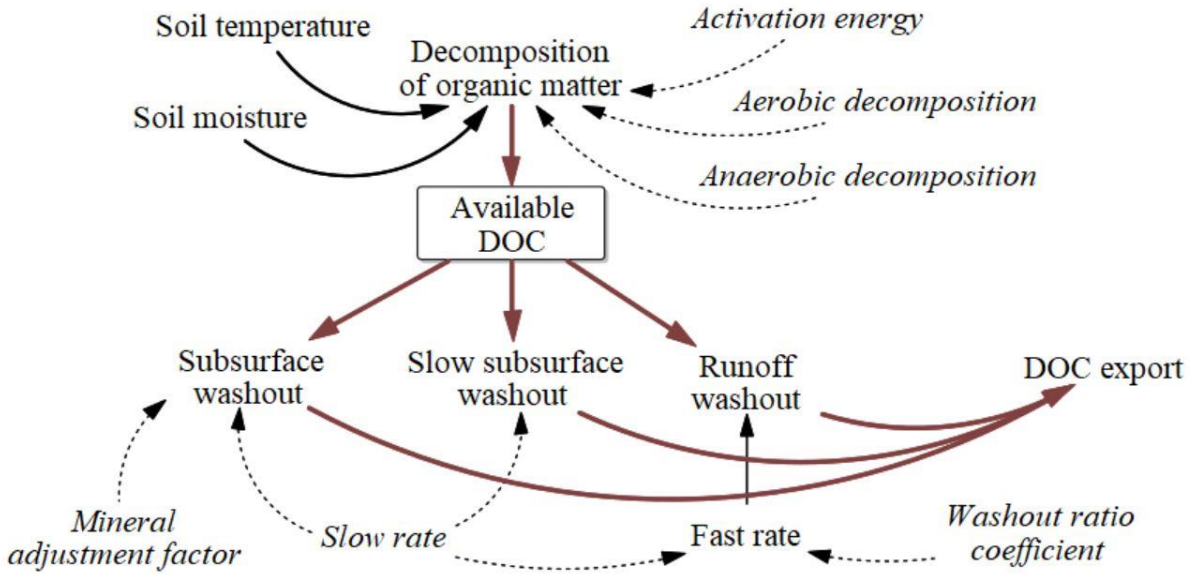

Figure 2 Overview of the DOC model. Soil moisture and soil temperature are driving the decomposition, indicated with black arrows. The output is DOC export as streamflow concentration or DOC load. The brown arrows indicate the transport of DOC and its direction. The box indicates DOC storage and the parameters in normal font are DOC fluxes. Dashed arrows are catchments specific parameters and parameters in italics are either calculated or calibrated.

Table 2 Catchment specific DOC parameters where each parameter represents an average over the whole catchment, shown in italics in figure 2. All parameters were calibrated except for the activation energy which was derived from literature.

DOC parameters	Explanation
Anaerobic decomposition	DOC production through anaerobic decomposition (gC m^{-2} day^{-1})
Aerobic decomposition	Rate of change in DOC production affected by soil moisture
Slow rate	Slow rate of DOC washout from subsurface flow (fraction cm^{-1})
Washout ratio coefficient	Adjusts the fast rate of washout, dependent on the slow rate (fraction)
Mineral adjustment factor	Accounts for processes affecting washout in mineral soils
Activation Energy	Energy needed to start decomposition reaction

2.2 Study area

Lake Mälaren is the third largest lake in Sweden and an important drinking water source. It is the main drinking water supply for the capital of Stockholm where it supplies over 2.2 million people in the area with drinking water (Norrvatten n.d.; Stockholm Vatten och Avfall n.d.), but additional cities around the lake also rely on it for drinking water.

Mälaren catchment covers an area of 21 507 km^2, which corresponds to almost 5% of the total area of Sweden. The lake is fed by twelve larger inflows as well as smaller streams located close to the lake (Wallin et al. 2000). This study examines hydrology and DOC export of 13 sub catchments that drain into the Galten and Ekoln basins through the rivers Arbågaån, Hedströmmen, Köpingsån and Fyrisån, as well as the smaller inflows Hågaån, Sävaån and Örsundaån (table 3; figure 3). Two study catchments, Kringlan and Vattholma, are smaller catchments located within the larger catchments Hammarby and Ulva Kvarndamm. This gave the possibility to evaluate how well hydrology and DOC responses from smaller catchments can be scaled up. Kolbäcksån is an important inflow to the Galten basin but was not included in this study since it is a highly regulated river, making it more complicated to model.

The study catchments are located in the western and north-eastern parts of the Mälaren catchment (figure 3). Land cover and soil types vary between the different catchments (table 4 & 5). The western catchments that drain into the lake basin Galten generally have a larger percentage of forest and the eastern catchments that drain into the lake basin Ekoln have a larger percentage of arable land.

The lake water retention time increases as the water moves from west to east and north to south, where the lake outlets are located. The shortest retention time is found in the western basin Galten with only 0.07 years whereas the Ekoln basin has a retention time of 1.2 years (Wallin et al. 2000). The retention time and land cover of the catchment draining into each basin has a large effect on the water quality and the organic content of the water.

Table 3 Main inflows to the Galten and Ekoln basins and the studied catchments, as well as the water contribution of each catchment to the total basin and lake water volume. Based on Wallin et al. (2000).

Main inflows	Study catchments	Water contribution to basin volume	Water contribution to total lake volume
Galten			52%
Arbogaån	*Dalkarlshyttan, Kåfalla, Hammarby, Kringlan*, Fellingsbro*	48%	25%
Kolbäcksån		33%	17%
Hedströmmen	*Dömsta*	14%	7%
Köpingsån	*Odensvibron*	2%	1%
Local area		3%	2%
Ekoln			16%
Fyrisån	*Ulva Kvarndamm, Vattholma*, Sävja*	48%	8%
Örsundaån	*Härnevi*	18%	3%
Oxundaån		6%	1%
Märstaån		2%	0.3%
Local area	*Lurbo, Ransta*	26%	4%

* Kringlan is part of the larger catchment Hammarby and Vattholma is part of the larger catchment Ulva Kvarndamm

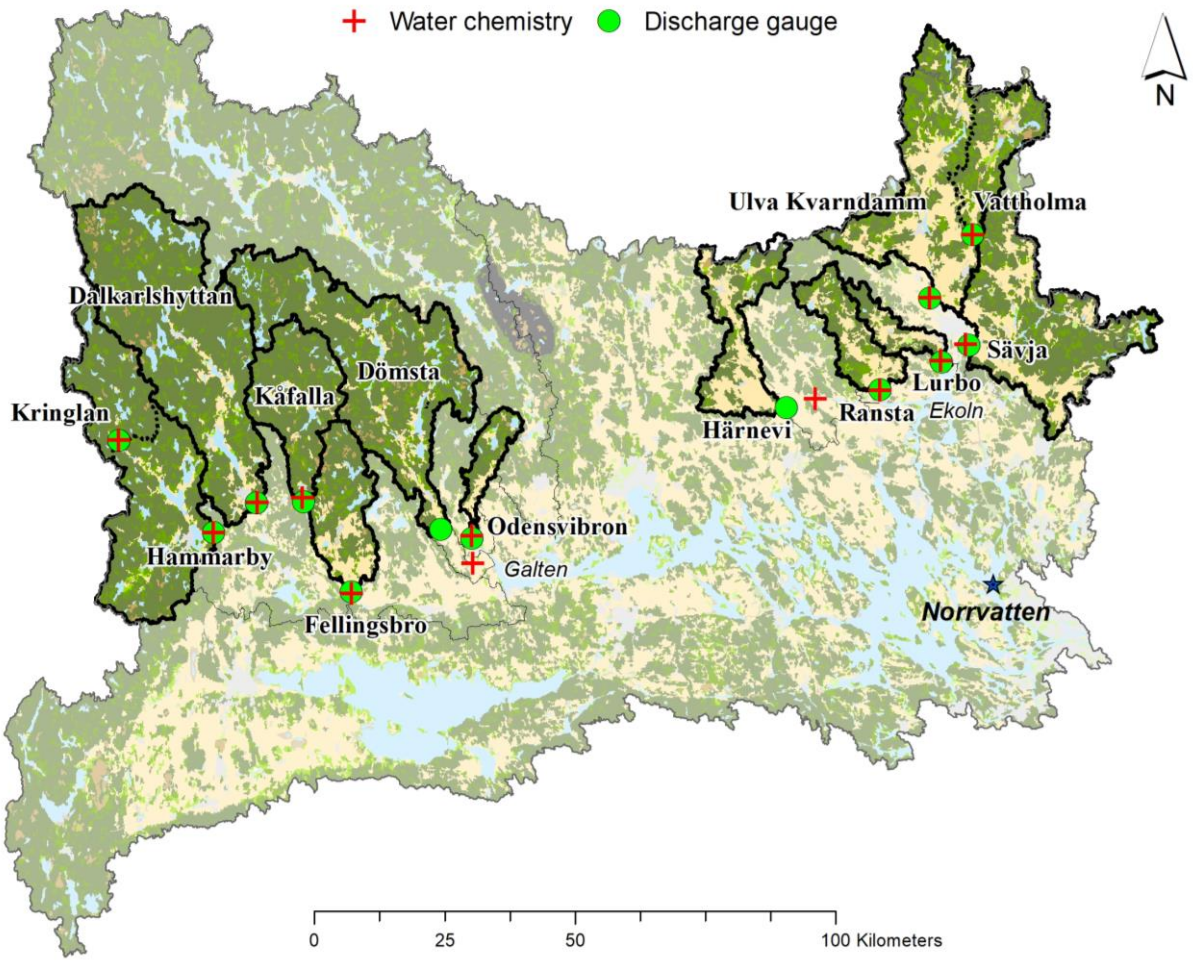

Figure 3 The entire Mälaren catchment outlined. Study areas are delineated with thick black lines, and the larger catchments they are part of are delineated with thinner lines. Kringlan and Vattholma are delineated with dashed lines as they are part of the larger catchments Hammarby and Ulva Kvarndamm. Discharge gauges and water chemistry locations, explained further in 2.3.2, are marked by green circle and red cross. Norrvatten drinking water treatment plant is marked with a star. Slightly transparent areas are not used in this study.

Table 4 Dominating soil types in each study catchment. Categories have been grouped to get a better overview. Based on soil map from the Swedish Geological Survey, SGU, scale 1:25 000-1:100 0000. Names in regular font are catchments for the larger inflows to Galten and Ekoln and names in italics are the smaller study catchments.

Catchment	Area (km^2)	Till	Clay-Silt	Peat	Glaciofluvial deposits	Water	Bedrock
Arbogaån	3802						
Dalkarlshyttan	1177	55%	8%	9%	2%	8%	16%
Kåfalla	388	46%	12%	13%	6%	6%	17%
Hammarby	888	51%	8%	9%	2%	10%	20%
*Kringlan**	293	46%	1%	12%	1%	8%	31%
Fellingsbro	297	41%	29%	15%	2%	6%	7%
Hedströmmen	1058						
Dömsta	994	45%	12%	12%	2%	9%	20%
Köpingsån	284						
Odensvibron	108	38%	37%	12%	-	7%	5%
Fyrisån	1982						
Ulva Kvarndamm	952	45%	34%	12%	2%	3%	3%
*Vattholma**	261	53%	20%	16%	1%	4%	6%
Sävja	735	39%	33%	8%	1%	2%	17%
Hågaån	123						
Lurbo	106	24%	43%	7%	-	1%	21%
Sävaån	200						
Ransta	197	33%	44%	8%	1%	1%	12%
Örsundaån	735						
Härnevi	327	40%	44%	6%	1%	1%	6%

Table 5 Total area of each main inflow and study catchment. Land cover as percentages for each catchment, based on CORINE land cover inventory. Some smaller categories have been grouped together for a better overview. Names in regular font are catchments for the larger inflows to Galten and Ekoln and names in italics are the smaller study catchments.

Catchment	Area (km^2)	Agriculture	Coniferous forest	Mixed & broad-leaved forest	Transitional woodland-shrub	Peat bogs
Arbogaån	3802					
Dalkarlshyttan	1177	5%	72%	5%	6%	2%
Kåfalla	388	5%	76%	2%	8%	3%
Hammarby	888	5%	70%	10%	3%	1%
Kringlan	293	1%	83%	5%	3%	1%
Fellingsbro	297	23%	55%	3%	8%	4%
Hedströmmen	1058					
Dömsta	994	7%	68%	6%	7%	3%
Köpingsån	284					
Odensvibron	108	20%	58%	5%	8%	2%
Fyrisån	1982					
Ulva Kvarndamm	952	32%	42%	10%	9%	1%
Vattholma	261	17%	48%	10%	15%	3%
Sävja	735	29%	55%	8%	4%	-
Hågaån	123					
Lurbo	106	29%	56%	4%	2%	-
Sävaån	200					
Ransta	197	33%	51%	9%	5%	-
Örsundaån	735					
Härnevi	327	40%	47%	5%	4%	1%

2.3 Data collection

All data used in this study are open-access and were downloaded in January and February 2022. Data was obtained from the European Climate Assessment & Dataset Project (ECA&D) and Copernicus Land Monitoring Service, The Inter-Sectorial Impact Model Intercomparison Project (ISIMIP), the Swedish Meteorological and Hydrological Institute (SMHI), the Swedish Agricultural University (SLU) and the Swedish Geological Survey (SGU). All data used is further described below.

2.3.1 Temperature and precipitation

Gridded data of past daily mean air temperature (°C) and precipitation (mm day^{-1}) was obtained from the E-OBS database at a 0.1-degree horizontal resolution (Haylock et al. 2008). The data is based on observations and was available from 1950-2021. A temperature and precipitation spatially weighted average was calculated for each catchment.

Future temperature and precipitation data were obtained from the open access ISIMIP2b simulation round. Representative Concentration Pathways (RCP) scenarios 2.6, 6.0 and 8.5 and four different bias corrected global circulation models (GCM's) were available, GFDL-ESM2M, HadGEM2-ES, IPSL-CM5A-LR and MIROC5. All data had a 0.5-degree horizontal resolution and were available for the period 2006-2099 (Frieler et al. 2017). Relative to a historical reference calculated between 1986-2005, the global mean temperature in 2016-2035 is projected to increase by 0.3-0.7 °C for all three RCP scenarios. By 2081-2100, RCP2.6 is projected to increase by 0.3-1.7 °C, RCP6.0 by 1.4-3.1 °C and RCP8.5 by 2.6-4.8 °C (IPCC 2014). Historical temperature and precipitation were also downloaded from ISIMIP for the period 1950-2005 and used to obtain a reference period based on each individual GCM and with the same data resolution. Temperature was converted from K to °C and precipitation from kg m^{-2} s^{-1} to cm day^{-1}, and a spatially weighted average was calculated for each catchment. All temperature and precipitation data were downloaded as NetCDF-files and extracted using RStudio.

2.3.2 Streamflow and water chemistry

Streamflow was downloaded from the SMHI 'Water web' (Vattenwebb). The website provides measured stream discharge from discharge gauges across Sweden. The location of each discharge gauge was used to delineate the study catchments using ArcGIS (figure 3). The maximum available continuous period for each catchment was used to calibrate the model with a period of 10 years at the end of the available periods excluded to use as a validation period (table 6). For both calibration and validation, a one-year warm-up period was used to allow the model to stabilise, using original data.

Table 6 Gauged area, discharge station ID used by SMHI, calibration and validation period used for each catchment

	Gauged area (km^2)	Discharge station	Calibration period	Validation period
Arbogaån				
Dalkarlshyttan	1183	2206	1980-2011	2012-2021
Kåfalla	41	1532*	1966-1990	1991-2000
Hammarby	891	2153	1951-2011	2012-2021
Kringlan	295	2229	1980-2011	2012-2021
Fellingsbro	298	2205	1980-2011	2012-2021
Hedströmmen				
Dömsta	998	2219	1980-2011	2012-2021
Köpingsån				
Odensvibron	110	2221	1966-2011	2012-2021
Fyrisån				
Ulva Kvarndamm	976	2246*	1980-1989	1990-1999
Vattholma	294	2244	1980-2011	2012-2021
Sävja	722	2243*	1980-2010	2011-2020
Hågaån				
Lurbo	106	2245*	1980-1990	1991-2000
Sävaån				
Ransta	197	2247	1980-2011	2012-2021
Örsundaån				
Härnevi	327	2248	1980-2011	2012-2021

*Discharge stations have been discontinued

Water chemistry measurements are regularly undertaken by the Swedish Agricultural University (SLU) as a part of the Swedish environmental monitoring program and the data is made publicly available. Based on the location of the discharge gauge for each study catchment, a corresponding location for measurements of water chemistry was identified. Locations were found very close to discharge stations for all study catchments except for Dömsta and Härnevi, where the water chemistry measurements were located further downstream (figure 3). It is assumed that the DOC concentrations at these sites do not differ significantly from DOC concentrations at the discharge stations. As no DOC measurements were available, measurements of total organic carbon (TOC) (mg l^{-1} C) were primarily used as a proxy. This was supported by 5 years of measurements of DOC and TOC in Ulva Kvarndamm, where a linear regression between DOC and TOC gave TOC=0.95*DOC + 1.4 and R^2=0.93 ($p < 0.00001$). In some cases, Abs420 or Pt l^{-1} measurements of filtered water were available in longer time series than the TOC, which are two different ways to measure the brownness of the water. Then, a linear relationship between an overlapping period of TOC and Abs420 was used to transform Abs420 to TOC. In the cases where Pt l^{-1} was used, it was converted to Abs420 by using the relationship Pt mg $l^{-1} \approx 500 \times$ Abs420 (SLU 2022). A summary of available water chemistry data for each sub catchment is found in table 7. Despite some uncertainties connected to the transformation of Abs420 and Pt l^{-1} to TOC, the value of a longer time series of DOC proxies that could be used for calibration of the model was judged to outweigh these. Due to the low frequency of DOC data, it was decided to only use a calibration period, in order to obtain as good of a result as possible.

Table 7 Periods when data for DOC proxies in stream water were available for each study catchment and the frequency of the measurements, which is twice a month, monthly or bimonthly (every other month). Data was obtained from SLU.

	TOC	Colour	Frequency of measurements
Arbogaån			
Dalkarlshyttan	1993-2012		Bimonthly
Kåfalla	1987-2011	1968-1975; 1982-1986	Monthly
Hammarby	1997-2019		Bimonthly
Kringlan	2001-2012	1985-2000	Monthly
Fellingsbro	1993-2019		Bimonthly
Hedströmmen			
Dömsta		1965-1995	Monthly
Köpingsån			
Odensvibron	2009-2010	2006-2008	Monthly
Fyrisån			
Ulva Kvarndamm	1994-1996	1985-1990*	Bi-monthly
Vattholma	1991-2021		Monthly
Sävja	1993-2021	1965-1992	Monthly
Hågaån			
Lurbo	2003-2004	1985-2002*	Twice a month; Bimonthly
Sävaån			
Ransta	2003-2005	1985-2002*	Monthly; Bimonthly
Örsundaån			
Härnevi	1965-2010		Monthly

*Abs420 converted from mg Pt l^{-1}

2.3.3 Land cover and soil types

Land cover for each study catchment was obtained from CORINE land cover inventory mapped in 2018. The maps are based on satellite images with a resolution of 10×10 to 25×25 m. The same land cover was used for the whole study period, even though some changes will have occurred during the period. The land cover classes that cover a minimum of one percent of at least one catchment are summarised in table 5. Agriculture includes a mixture of arable land and pasture, coniferous forests are dominated by spruce and pine, broad-leaved forest by birch, and mixed forest by spruce, pine and birch; transitional woodland-shrub include young forest and clear-cuts, both in and outside wetland areas; peat bogs include peat producing wetlands that have less than 30% tree or shrub cover. Soil maps were downloaded from the Swedish Geological Survey (SGU) and summarised for each catchment (table 4).

2.4 Model calibration

Automated multi-step calibration methods were developed to calibrate all 13 catchments for both the hydrology and DOC model. The calibration sequence was developed to best represent the function of each parameter by minimising the root mean square error between measured and simulated variables, as was done by Schneiderman et al. (2009). The optimum parameter value found at each step was used to run the simulation for the next calibration step. Measured streamflow was divided into runoff and baseflow according to the baseflow separation method described by Arnold et al. (1995) and used in the calibration process. Performance of calibration and validation periods were analysed with the goodness-

of-fit metrics Nash-Sutcliffe efficiency (NSE) and R^2. NSE values range from 1 to -∞, where 1 means a perfect fit and negative values mean that the observed mean would perform better (Nash and Sutcliffe, 1970). The goodness-of-fit was evaluated on daily discharge during calibration and validation, DOC concentrations for the calibration period as well as daily and monthly DOC loads, based on interpolated values, for the periods with overlapping DOC and discharge measurements. The optimal parameter values found were analysed for correlation with land cover and soil types by linear regression. Vattholma and Kringlan, two catchments with contrasting caracteristics, were chosen for a sensitivity analysis of all hydrologic and DOC calibrated parameters, except for the aerobic decomposition coefficient which had a range derived from literature, to check for equifinality. All parameters were kept constant at their optimised value except for the parameter being analysed. This parameter was set to increase within the range used during optimisation, from the minimum value up to the maximum with approximately 200 steps.

2.4.1 Hydrological calibration

The hydrological parameters were calibrated through following six steps which were then repeated in a second iteration: the precipitation correction factor was optimised to a water balance equation of measured streamflow and potential evapotranspiration; the curve number adjustment factor to cumulative measured and simulated runoff; the melt coefficient to measured and simulated streamflow; the recession coefficient and soil water capacity to measured and simulated baseflow; the slow recession coefficient and deep soil water capacity to the 20^{th} percentile of measured and simulated baseflow; the channel flow coefficient to measured and simulated runoff. Both recession coefficients were then optimised together once the soil water capacity and deep ground water capacity, that defines the relative importance of the two recession coefficients, had been determined by comparison of measured and simulated streamflow. Finally, the precipitation correction factor was optimised one last time to a water balance equation based on simulated actual evapotranspiration and measured streamflow. Simulated evapotranspiration was also used in the first step of the repeat of the optimisation sequence.

2.4.2 DOC calibration

The DOC calibration was conducted in 8 steps in total: the anaerobic decomposition coefficient, slow rate and washout ratio coefficient were calibrated by comparison of simulated and measured DOC concentrations; the anaerobic decomposition coefficient by comparison with measured DOC concentrations when water content in the unsaturated zone was close to soil water capacity; aerobic decomposition coefficient to DOC concentrations when the unsaturated zone is below soil water capacity; mineral adjustment factor by comparison with all measured DOC concentrations. Step two to four were then repeated to reoptimize the anaerobic decomposition coefficient, aerobic decomposition coefficient and mineral adjustment coefficient.

2.5 Climate scenario simulations

Using the calibrated parameters, the model was run for each catchment with temperature and precipitation data from all three future climate scenarios and the historical reference period for all four GCM's. Hydrological and DOC responses of interest was then extracted from the model. Hydrological responses included snowfall, evapotranspiration, growing days, streamflow, baseflow, runoff, unsaturated, saturated and deep saturated zones. Responses from the DOC-model included soil temperature, DOC concentration and DOC load. Mean annual values were calculated for each simulated response and the historical mean for the period 1961-1990 was subtracted from this to obtain the anomaly. Monthly anomalies were also calculated by subtracting the mean value for each month. A linear regression analysis was done on simulated DOC concentrations and loads with land cover.

2.6 DOC loads

DOC concentration measurements from SLU were linearly interpolated between measurements. Concentrations were then multiplied with the daily discharge measurements to calculate measured daily and monthly DOC loads for the periods of overlapping DOC and discharge measurements for each catchment. The daily simulated DOC and streamflow were used to calculate simulated daily, monthly, and annual DOC loads. Total loads from the Galten and Ekoln catchments were summed to calculate changes in annual and monthly DOC loads to the basins from the study catchments. Kringlan and Vattholma were excluded from this as they are part of the larger catchments Hammarby and Ulva Kvarndamm. An assumption was made that the DOC loads simulated at each catchment outlet would represent the load to lake basins, despite some degradation that could occur during in-stream transport.

3 Results

3.1 GWLF-Hydrology model performance

Model performance was evaluated by the statistical goodness of fit measures Nash-Sutcliffe efficiency (NSE) and R^2, as well as visual inspection of the hydrographs. Calibration and validation periods generally showed similar values, with approximately as many catchments performing better during calibration as during validation (table 8 & 9). Simulated streamflow showed a good performance in all catchments with NSE in the validation periods of 0.59-0.77 and R^2 of 0.61-0.79. Some measured peaks were missed by the simulation, and the falling limb of the hydrograph was not completely replicated (figure 4). However, comparison with HYPE-simulated streamflow also showed difficulties in replicating some of these flow peaks. Baseflow performance in most catchments was generally slightly lower than for streamflow, with validation NSE of 0.56-0.82 and R^2 of 0.62-0.85, although some catchments performed better. The same problem was seen in capturing the falling limb as in streamflow (figure 4). All catchments showed the lowest model performance for simulated runoff, with validation NSE that ranged between 0.20-0.59 and R^2 of 0.28-0.61. Simulated runoff missed some peaks which was more pronounced in some catchments, as in Fellingsbro (figure 4).

Table 8 Goodness-of-fit values for calibration of each catchment. Different time periods were used, specified in table 6. NSE and R^2-values are reported for total streamflow, which is the combined baseflow and runoff, as well as for baseflow and runoff, obtained from hydrograph separation.

Calibration	*Streamflow*		*Baseflow*		*Runoff*	
	NSE	*R^2*	*NSE*	*R^2*	*NSE*	*R^2*
Arbogaån						
Dalkarlshyttan	0.65	0.66	0.64	0.66	0.36	0.40
Kåfalla	0.64	0.64	0.54	0.55	0.50	0.51
Hammarby	0.71	0.73	0.66	0.70	0.44	0.47
Kringlan	0.72	0.73	0.67	0.72	0.48	0.50
Fellingsbro	0.68	0.70	0.70	0.73	0.39	0.43
Hedströmmen						
Dömsta	0.67	0.69	0.68	0.72	0.37	0.40
Köpingsån						
Odensvibron	0.58	0.59	0.63	0.67	0.23	0.29
Fyrisån						
Ulva Kvarndamm	0.72	0.74	0.66	0.72	0.42	0.47
Vattholma	0.76	0.77	0.71	0.75	0.38	0.40
Sävja	0.66	0.68	0.59	0.66	0.39	0.42
Hågaån						
Lurbo	0.69	0.70	0.69	0.72	0.43	0.47
Sävaån						
Ransta	0.62	0.64	0.54	0.65	0.37	0.40
Örsundaån						
Härnevi	0.60	0.61	0.56	0.64	0.35	0.38

Table 9 Goodness-of-fit values for validation of each catchment. NSE and R^2-values are reported for total streamflow, which is the combined baseflow and runoff, as well as for baseflow and runoff, obtained from hydrograph separation. All validation periods are 10 years, specified in table 6.

Validation	*Streamflow*		*Baseflow*		*Runoff*	
	NSE	R^2	*NSE*	R^2	*NSE*	R^2
Arbogaån						
Dalkarlshyttan	0.64	0.64	0.68	0.69	0.27	0.33
Kåfalla	0.61	0.62	0.60	0.62	0.41	0.43
Hammarby	0.70	0.73	0.71	0.78	0.27	0.31
Kringlan	0.68	0.72	0.68	0.76	0.31	0.35
Fellingsbro	0.77	0.78	0.82	0.85	0.35	0.38
Hedströmmen						
Dömsta	0.74	0.75	0.73	0.78	0.34	0.40
Köpingsån						
Odensvibron	0.59	0.61	0.74	0.75	0.25	0.28
Fyrisån						
Ulva Kvarndamm	0.67	0.72	0.56	0.70	0.28	0.32
Vattholma	0.72	0.74	0.70	0.73	0.42	0.45
Sävja	0.75	0.79	0.64	0.75	0.59	0.61
Hågaån						
Lurbo	0.63	0.65	0.67	0.70	0.20	0.28
Sävaån						
Ransta	0.69	0.70	0.61	0.71	0.43	0.45
Örsundaån						
Härnevi	0.69	0.69	0.66	0.71	0.45	0.45

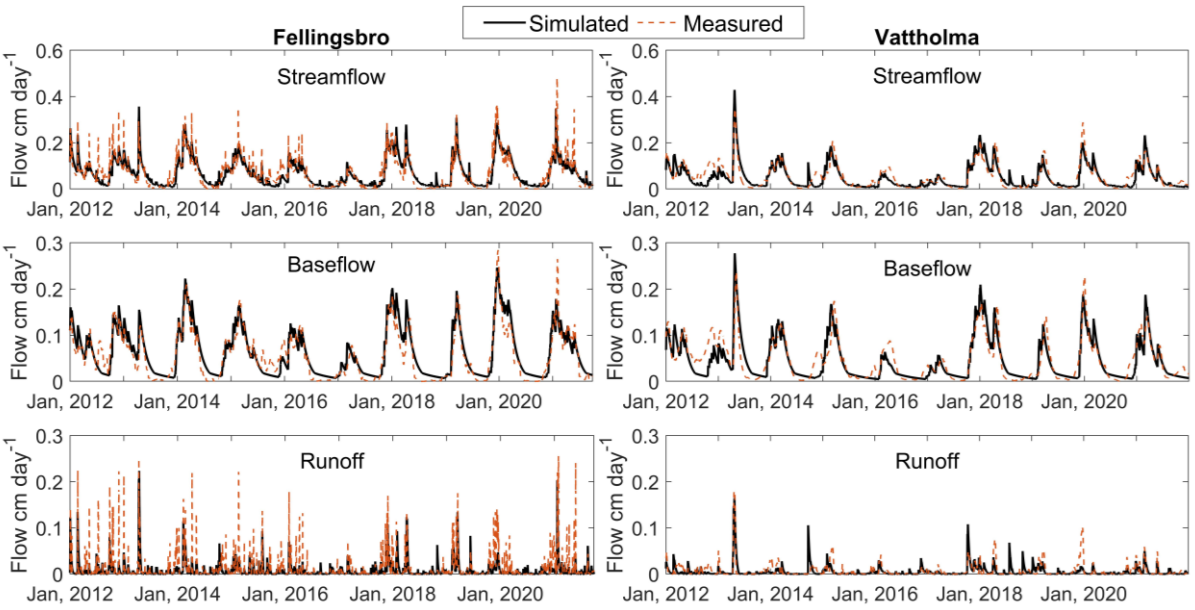

Figure 4 Simulated (black) and measured (dashed orange) streamflow (top), baseflow (middle) and runoff (bottom) for validation periods of Fellingsbro (left) and Vattholma (right). Graphs of the other catchments can be found in appendix 1.

A linear regression analysis was done for all optimised parameters (table 10) and catchment characteristics (figure 5 & 6). The parameters *CN-adjustment factor*, *channel flow coefficient*, *recession coefficient* and *slow recession coefficient* showed a significant correlation with soil types and land cover (p-value <0.05). CN-adjustment factor and channel flow coefficient showed a similar correlation to soil types, with decreasing values as the areal extent of till, water and peat increased. In addition, both parameters increased with an increase of clay-silt cover. The value of the recession coefficient also

increased with larger clay-silt cover whereas the slow recession coefficient decreased. The recession coefficient presented significant correlation with the most soil types. It decreased as the cover of till, water, peat and glaciofluvial deposits increased. The slow recession coefficient was the only parameter that correlated to bedrock cover. Although removing Kringlan, which has the highest proportion of bedrock (30%), the correlation was no longer significant.

Regarding the land cover, CN-adjustment factor values correlated with transitional woodland shrub, with decreasing values as the land cover increased (figure 6). The value of the channel flow coefficient decreased with larger area of coniferous forest but increased with agricultural area. Larger area of peat bogs and coniferous forest also decreased the value of the recession coefficient but increased with agricultural area. Lastly, the slow recession coefficient decreased as the agricultural area increased, and increased with increased areal cover of coniferous forest.

No correlation could be found between catchment caracteristics and streamflow performance through a regression analysis. Performance of simulated runoff was increasing with increasing areal cover of bedrock (R^2=0.29; p=0.04) and performance of simulated baseflow was decreasing with increased areal cover of glacioflucial deposits (R^2=0.24; p=0.05). From the sensitivity analysis conducted on Kringlan and Vattholma, none of the parameters showed equifinality.

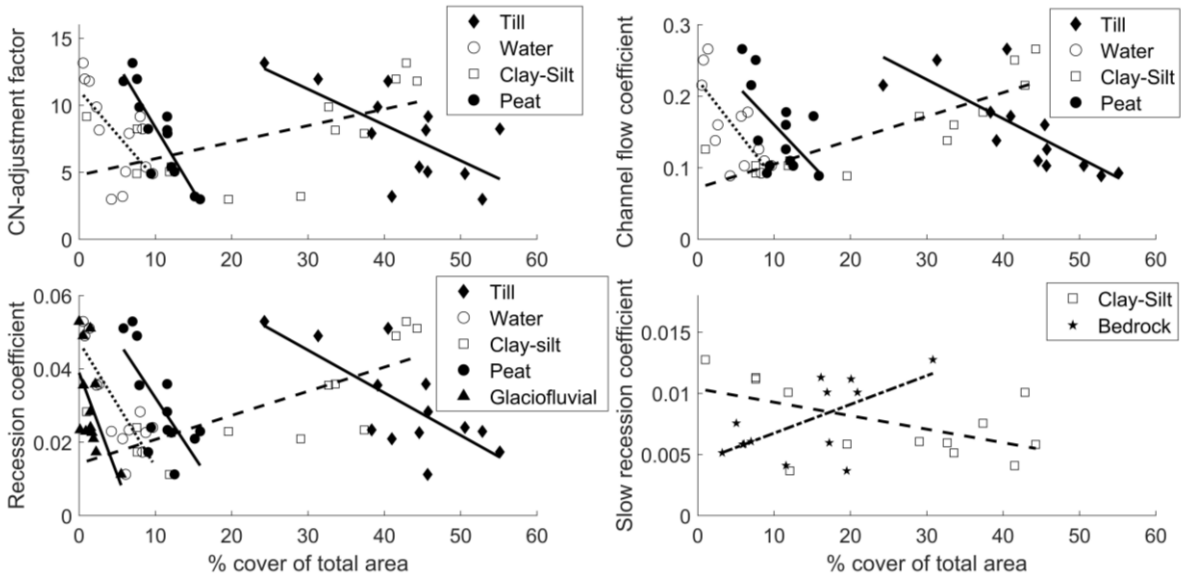

Figure 5 Significant correlation (p<0.05) between areal extent of soil types and four calibrated parameters: (top left) CN-adjustment factor (Till: R^2=0.40, p=0.01, Water: R^2=0.35, p=0.02, Clay-Silt: R^2=0.26, p=0.04, Peat: R^2=0.73. p=0.0001); (top right) channel flow coefficient (Till: R^2=0.56, p=0.002, Water: R^2=0.51, p=0.004, Clay-Silt: R^2=0.71, p=0.0002 , Peat: R^2=0.27, p=0.04); (bottom left) recession coefficient (Till: R^2=0.49, p=0.005, Water: R^2=0.63, p=0.0007, Clay-Silt: R^2=0.52, p=0.003, Peat: R^2=0.47, p=0.006, Glaciofluvial deposits: R^2=0.28, p=0.04); (bottom right) slow recession coefficient (Clay-Silt: R^2=0.25, p=0.05, Bedrock: R^2=0.35, p=0.02). Each symbol represents the calibrated value for one catchment and its areal percentage of soil types.

Table 10 Parameter values obtained from calibration, except the ET restriction coefficient that was calculated based on literature values and catchment specific land cover.

	Precipitation correction factor	Melt coefficient	CN-adjustment factor	Channel flow coefficient	ET restriction coefficient	Soil water capacity	Recession coefficient	Deep soil water capacity	Slow recession coefficient
Calibration range	0.5-1.5	0.05-0.6	-30-30	0.01-1	calculated	1-20	0.005-0-3	1-8	0.001-0.1
Arbogaån									
Dalkarlshyttan	1.07	0.22	8.23	0.09	0.66	9.87	0.017	3.09	0.011
Kåfalla	1.22	0.29	5.05	0.10	0.67	16.10	0.011	2.95	0.010
Hammarby	1.13	0.19	4.90	0.10	0.66	17.01	0.024	2.94	0.011
Kringlan	1.07	0.19	9.16	0.13	0.68	13.86	0.028	2.95	0.013
Fellingsbro	1.14	0.20	3.20	0.17	0.64	16.47	0.021	2.97	0.006
Hedströmmen									
Dömsta	1.21	0.17	5.40	0.11	0.65	16.65	0.023	2.81	0.004
Köpingsån									
Odensvibron	1.20	0.20	7.90	0.18	0.65	18.89	0.023	3.15	0.008
Fyrisån									
Ulva Kvarndamm	0.98	0.15	8.15	0.16	0.62	15.10	0.036	3.23	0.005
Vattholma	1.06	0.18	2.99	0.09	0.62	17.85	0.023	2.97	0.006
Sävja	1.07	0.18	9.87	0.14	0.64	16.65	0.036	2.80	0.006
Hågaån									
Lurbo	1.28	0.20	13.15	0.22	0.65	13.26	0.053	2.96	0.010
Sävaån									
Ransta	1.21	0.20	11.96	0.25	0.64	16.08	0.049	2.97	0.004
Örsundaån									
Härnevi	1.21	0.24	11.80	0.27	0.64	16.33	0.051	2.89	0.006

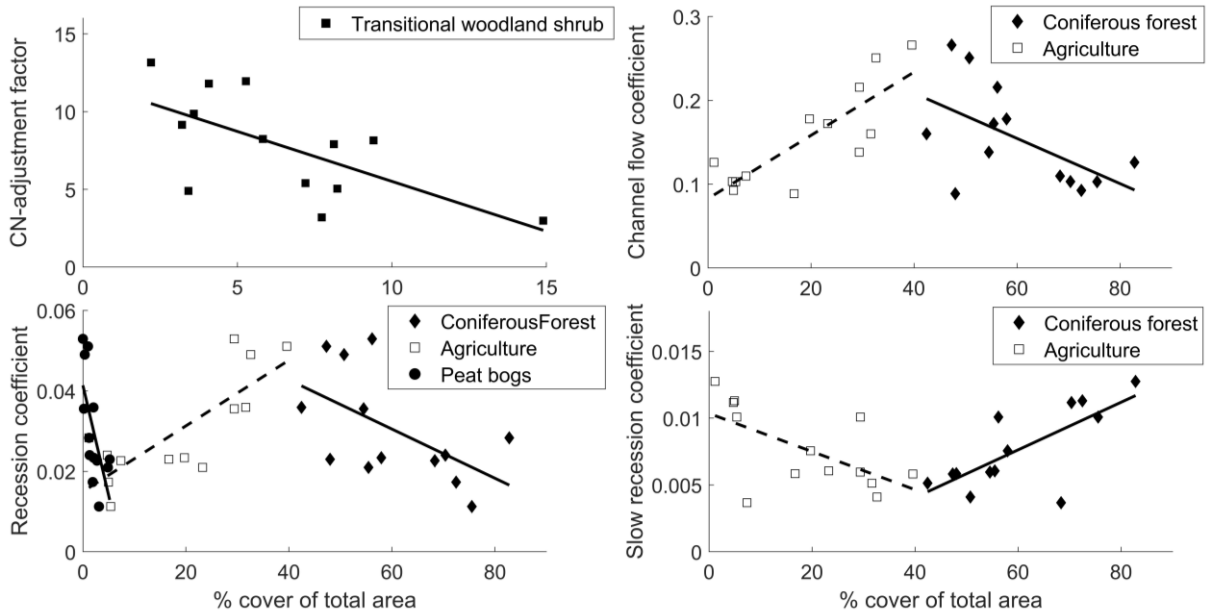

Figure 6 Significant correlation ($p<0.05$) between areal extent of land cover and four calibrated parameters: (top left) CN-adjustment factor (Transitional woodland shrub: $R^2=0.38$, $p=0.01$); (top right) channel flow coefficient (Coniferous forest: $R^2=0.25$, $p=0.05$, Agriculture: $R^2=0.65$, $p=0.001$); (bottom left) recession coefficient (Coniferous forest: $R^2=0.26$, $p=0.04$, Agriculture: $R^2=0.59$, $p=0.001$, Peat bogs: $R^2=0.39$, $p=0.01$); (bottom right) slow recession coefficient (Coniferous forest: $R^2=0.50$, $p=0.004$, Agriculture: $R^2=0.32$, $p=0.03$). Each symbol represents the calibrated value for one catchment and its areal percentage of land cover.

3.2 GWLF-DOC model performance

NSE-values of DOC concentrations, calculated from measuread and simulated concentrations at the time of measurements, showed an overall poor performance (table 11). Most catchments had a negative NSE, with only Kåfalla, Kringlan, Odensvibron and Vattholma showing positive values. R^2-values showed a better performance, but still generally low values. Nevertheless, the simulated variations in concentrations were generally consistent when compared to the range of measured concentrations (figure 7). Daily and monthly loads, based on periods of overlapping DOC and discharge measurements, showed a similar fit as the hydrology results. Better performance in simulated DOC concentrations was not necessarily associated with a better performance for simulated DOC loads. Instead, performance of simulated DOC loads was more strongly impacted by the performance of the hydrology simulations, showing the important impact of hydrological transport on DOC export. For example, Kåfalla had the second highest NSE for DOC concentrations and highest R^2. Despite this, it presented the lowest NSE and among the lowest R^2 for DOC loads. Regression analysis showed that several land covers and soil types were correlated with performance of simulated DOC concentrations. Catchment characteristics that increased performance of simulated DOC concentrations were coniferous forest ($R^2=0.27$, $p=0.04$), peat ($R^2=0.38$, $p=0.02$) and glaciofluvial deposits ($R^2=0.29$, $p=0.03$). Characteristics that decreased the performance were agricultural land ($R^2=0.45$, $p=0.007$) and clay-silt soil ($R^2=0.42$, $p=0.01$). Only till showed correlation with model performance on daily DOC loads, with increasing R^2 in catchments with higher till coverage ($R^2=0.42$, $p=0.01$).

Table 11 NSE and R^2 values for DOC concentration at measured points only, daily and monthly DOC loads based on interpolated DOC measurements and daily discharge measurements, as well as daily simulated DOC.

Calibration	DOC concentrations		Daily DOC loads		Monthly DOC loads	
	NSE	R^2	NSE	R^2	NSE	R^2
Arbogaån						
Dalkarlshyttan	-0.16	0.24	0.60	0.64	0.69	0.70
Kåfalla	0.32	0.50	0.25	0.59	0.42	0.66
Hammarby	-0.21	0.15	0.69	0.72	0.77	0.78
Kringlan	0.13	0.32	0.68	0.72	0.75	0.77
Fellingsbro	-0.05	0.14	0.46	0.58	0.57	0.66
Hedströmmen						
Dömsta	-0.23	0.26	0.39	0.65	0.54	0.74
Köpingsån						
Odensvibron	0.10	0.15	0.60	0.64	0.79	0.79
Fyrisån						
Ulva Kvarndamm	-0.98	0.09	0.73	0.74	0.81	0.83
Vattholma	0.35	0.37	0.73	0.76	0.76	0.78
Sävja	-0.92	0.26	0.61	0.63	0.63	0.66
Hågaån						
Lurbo	-0.32	0.11	0.50	0.64	0.66	0.74
Sävaån						
Ransta	-0.31	0.00	0.37	0.56	0.54	0.64
Örsundaån						
Härnevi	-1.28	0.05	0.46	0.57	0.68	0.71

Generally, the model captured the concentration range of measured data. Simulated concentrations showed a larger variation in Ekoln catchments, especially Sävja, Ransta, Lurbo and Härnevi with many drawdowns in concentrations (appendix 2). In Ransta and Lurbo, the simulated DOC did not manage to capture any peak DOC concentrations. Lower DOC concentrations occured more often in summer and fall, whereas the concentrations were at a higher and more stable levels during winter and spring with occasional peaks. Lower simulated concentrations generally coincided with lower simulated streamflow (figure 7). Simulated DOC concentrations during calibration for Fellingsbro (NSE=-0.05, R^2=0.14) and Vattholma (NSE=0.35, R^2=0.37) generally followed the measured concentrations, but some peaks in concentrations were not replicated (figure 7). Measured DOC concetrations in Fellingsbro and Vattholma covered approximately the same period (1993-2019 & 1991-2021) and both displayed a slight upward trend which was succesfully captured by the model. Comparing the first and last 5 years of the calibration periods in both catchments, concentrations increased from 12.9 to 15.1 mg L^{-1} in Fellingsbro and 15.3 to 21.1 mg L^{-1} in Vattholma. DOC measurements were made in the same months in both 5-year periods. In the same years, mean annual air temperature increased by 1.5 °C in Fellingsbro and 0.6 °C in Vattholma. Mean annual precipitation sum was unchanged in Fellingsbro and increased by only 10 mm $year^{-1}$ in Vattholma. Simulated DOC loads showed a better fit to measuread interpolated loads, and the fit got better for monthly compared to daily loads (table 11, figure 8). The peak in DOC concetration in Fellingsbro in 2001 was not captured by simulated concentration (figure 7) or by daily or monthly loads (figure 8). Similarly, there was a peak in concentrations in 2009 in Vattholma that was not completely captured by simulated concentrations or loads.

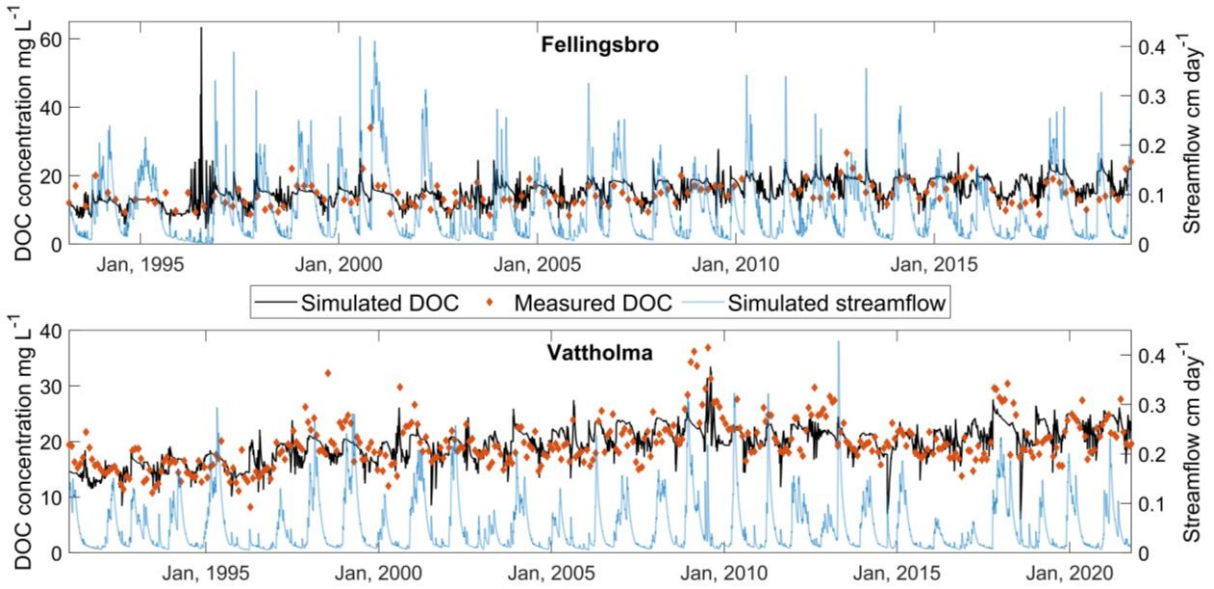

Figure 7 Simulated (black line) and measured (orange diamonds) DOC concentrations and simulated streamflow (blue line) for Fellingsbro (top) and Vattholma (bottom). Graphs for the other catchments can be found in appendix 2.

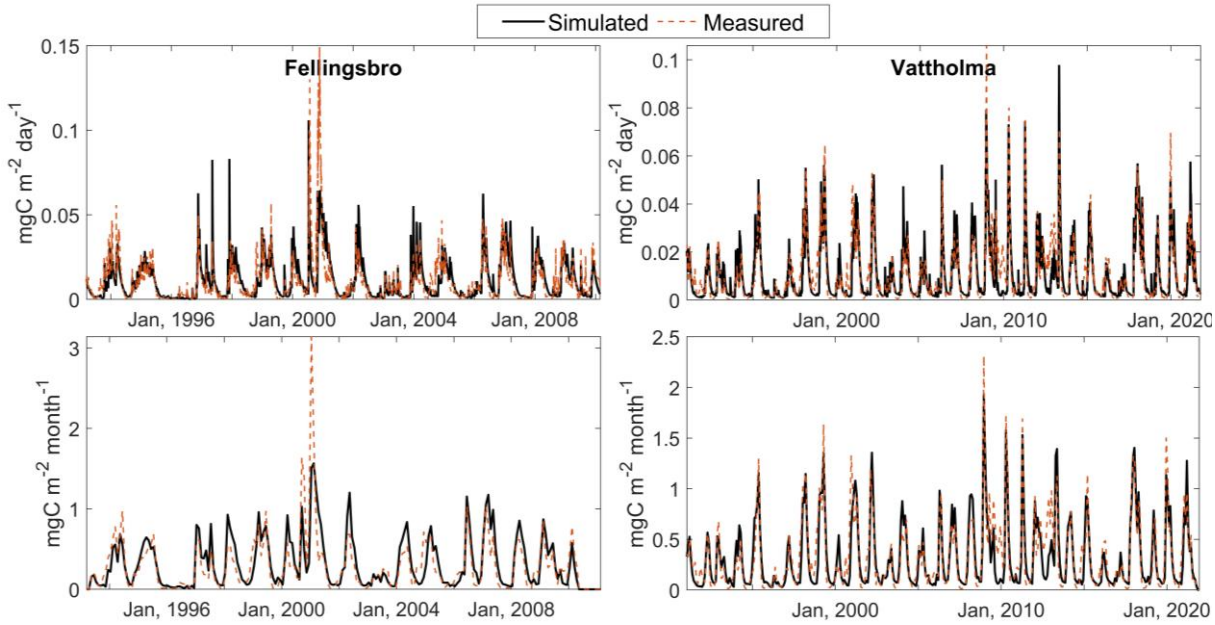

Figure 8 Daily (top) and monthly (bottom) simulated (black) and measured (dashed orange) DOC loads from Fellingsbro (top) and Vattholma (bottom). Measured loads are caluclated from interpolated measured DOC concentrations and daily streamflow. Graphs for the other catchments can be found in appendix 2.

Table 12 Obtained DOC parameters through optimisation, except for activation energy that was based on literature values averages over each catchment

	Activation Energy	Anaerobic decomposition	Aerobic decomposition	Slow rate	Washout ratio	Mineral adjustment
Range	literature	0.001-0.1	4-7	0.001-0.2	0.1-6	0.1-1
Arbogaån						
Dalkarlshyttan	5.9	0.017	5.7	0.0017	1.54	0.70
Kåfalla	5.8	0.021	4.0	0.0010	1.33	0.51
Hammarby	6	0.012	7.0	0.0025	1.13	0.87
Kringlan	6	0.015	7.0	0.0018	1.02	0.71
Fellingsbro	5.8	0.015	7.0	0.0025	1.99	0.64
Hedströmmen						
Dömsta	5.9	0.019	4.0	0.0010	2.23	0.67
Köpingsån						
Odensvibron	5.9	0.018	4.1	0.0066	2.04	0.83
Fyrisån						
Ulva Kvarndamm	5.9	0.009	7.0	0.0059	1.64	0.83
Vattholma	5.7	0.012	7.0	0.0050	1.68	0.82
Sävja	6	0.018	6.0	0.0020	1.87	0.56
Hågaån						
Lurbo	6	0.016	7.0	0.0056	1.08	0.70
Sävaån						
Ransta	6	0.011	6.6	0.0050	1.89	0.87
Örsundaån						
Härnevi	5.9	0.014	7.0	0.0038	2.20	0.87

A regression analysis was done on measured DOC concentrations and discharge for the calibration period for all catchments. All catchments showed a significant positive linear correlation ($p<0.05$) with increasing DOC concentration during higher flows. However, some with a very low R^2 which ranged 0.02-0.24, and for most catchments high DOC concentration could occur during both high and low flows. No relationship could be established between catchment characteristics and the relationship between DOC concentration and discharge.

All calibrated parameters (table 12) were analysed through a linear regression analysis with land covers and soil types. All parameters except for the aerobic decomposition coefficient showed correlations to some catchment characteristics (figure 9). Slow rate showed higher values in catchments with larger proportion of agriculture ($R^2=0.30$, $p=0.03$) and clay-silt ($R^2=0.43$, $p=0.01$), but values decreased as the area of coniferous forest ($R^2=0.43$, $p=0.01$), water ($R^2=0.25$, $p=0.05$), glaciofluvial deposits ($R^2=0.26$, $p=0.04$) and bedrock ($R^2=0.25$, $p=0.05$) increased. Larger areal extent of mixed and deciduous forest gave a higher mineral adjustment factor ($R^2=0.32$, $p=0.03$) and a lower anaerobic decomposition ($R^2=0.62$, $p=0.001$). The washout ratio decreased as areal cover of bedrock increased ($R^2=0.36$, $p=0.02$). A sensitivity analysis on all calibrated parameters was conducted on Kringlan and Vattholma, and found no equifinality.

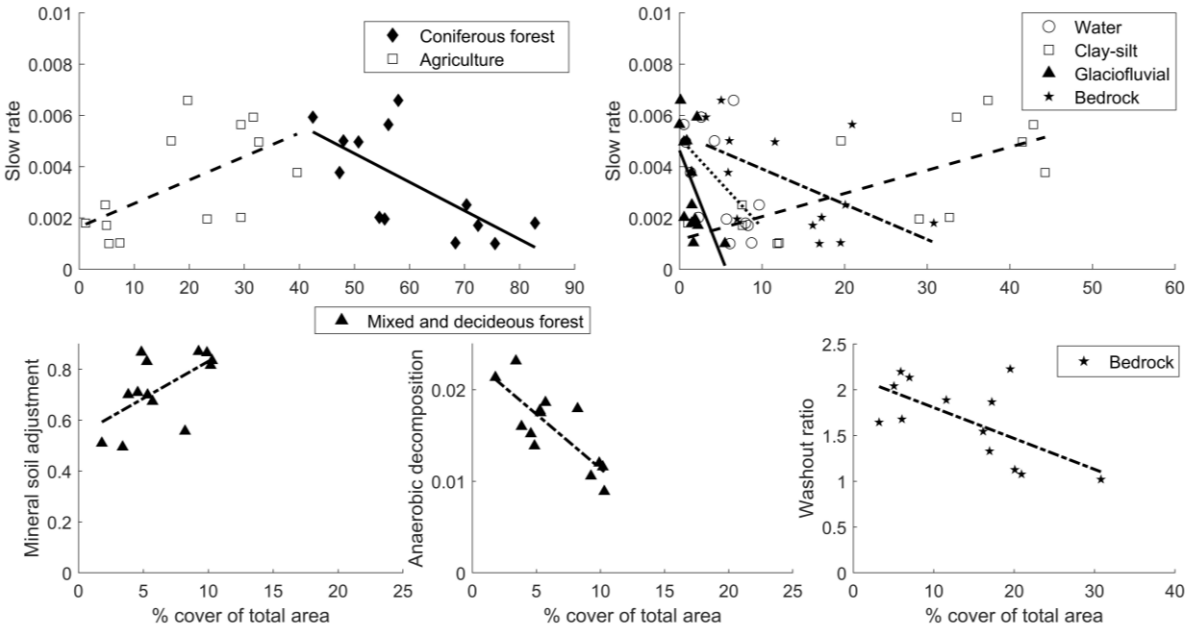

Figure 9 Significant correlations ($p<0.05$) between areal extent of soil and land cover and the calibrated DOC-model parameters slow rate, anaerobic decomposition, mineral adjustment factor, and washout ratio. Each symbol represents the calibrated value for one catchment and its areal percentage of land cover or soil types.

3.3 Future climate

Future climate was represented by three RCP-scenarios, RCP2.6, 6.0 and 8.5, and four GCM's providing daily precipitation and mean air temperature that were used to drive the GWLF-Hydrology-DOC model. In this section, future precipitation and air temperature from the four GCM's provided by ISIMIP are presented, whereas snowfall, growing days, evapotranspiration, and soil temperature were given as an output by the GWLF-model.

The mean annual precipitation sums for the reference period ranged between 623-778 mm year^{-1} in Galten and 584-636 mm year^{-1} in Ekoln. It increased over the coming century according to all RCP-scenarios and catchments (figure 10, table 13). There was a further increase in mean annual precipitation sum from 2040-2069 to 2070-2099 for all catchments. There was also a higher increase in mean annual precipitation with the higher RCP scenarios. The same overall annual and monthly behaviour could be seen in both Ekoln and Galten. As seen in figure 10, annual precipitation was not increasing linearly, but had periods with lower and higher precipitation. Overall, the winter months showed an increased median precipitation whereas the median precipitation during the summer months did not show a large difference under RCP2.6 and 6.0 but decreased slightly under RCP8.5. There was a large range in both annual and monthly precipitation, meaning that both increased and decreased precipitation is possible. During the reference period, the model simulated 21-28 % of the precipitation in Galten and 18-23 % in Ekoln as snowfall. In 2040-2069, this was 11-17 % in Galten and 9-11 % in Ekoln under RCP2.6, 9-15 % and 8-9 % under RCP6.0, and 7-13 % and 5-7 % under RCP8.5. In 2070-2099, the same amount of precipitation fell as snow under RCP2.6, 6-11 % and 5-6 % under RCP6.0, and 3-6 % and 2-3 % under RCP8.5.

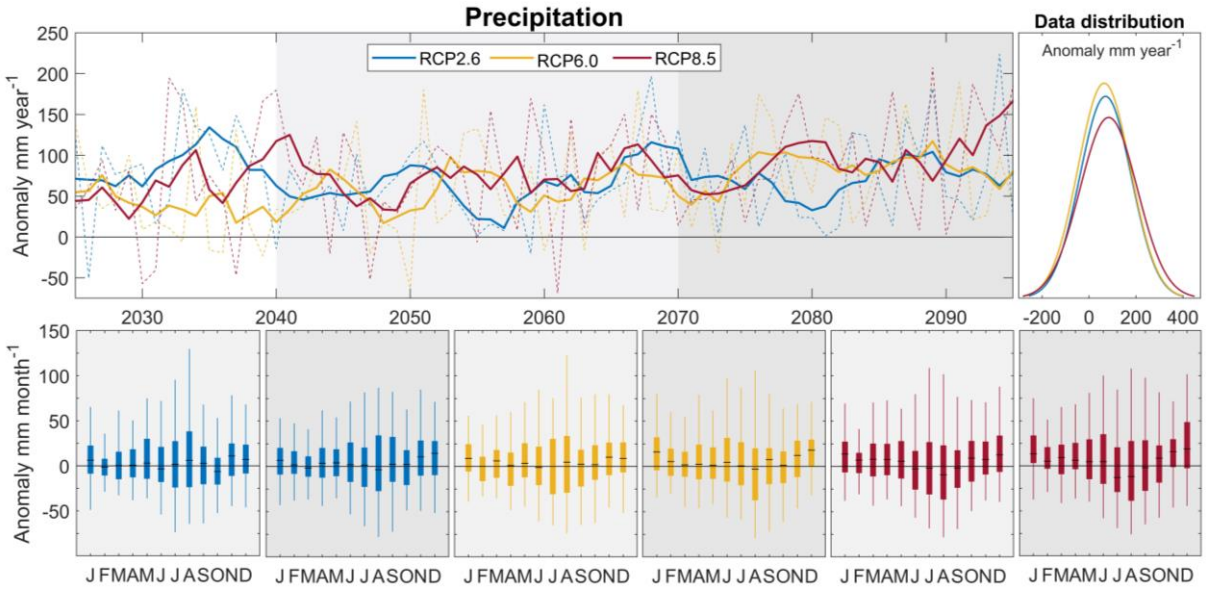

Figure 10 Precipitation anomalies for the whole Galten catchment. Top left: mean annual (dashed line) and 5-year moving average (solid line) for the three RCP scenarios compared to the reference period 1961-1990. Top right: Annual data distribution for the whole period, including all four GCM's. Bottom: Mean monthly anomaly for the period 2040-2069 (light grey) and 2070-2099 (darker grey), including the whole 30 year-periods and all four GCM's.

Table 13 Mean annual precipitation in mm year^{-1} for the reference period 1961-1990 and mean annual change in mm year^{-1} for the three RCP2.6, 6.0 and 8.5 in the periods 2040-2069 and 2070-2099. All four GCM's are used to calculate the mean.

Precipitation (mm year^{-1})	Reference	2040-2069			2070-2099		
	1961-1990	RCP2.6	RCP6.0	RCP8.5	RCP2.6	RCP6.0	RCP8.5
Arbogaån							
Dalkarlshyttan	732	+61	+58	+78	+70	+85	+107
Kåfalla	709	+66	+62	+84	+80	+96	+115
Hammarby	766	+56	+55	+75	+64	+78	+103
Kringlan	778	+56	+55	+74	+62	+76	+103
Fellingsbro	655	+61	+58	+78	+75	+90	+106
Hedströmmen							
Dömsta	664	+62	+59	+80	+76	+91	+108
Köpingsån							
Odensvibron	623	+56	+57	+73	+74	+87	+99
Fyrisån							
Ulva Kvarndamm	623	+60	+64	+80	+79	+96	+115
Vattholma	636	+62	+66	+83	+82	+100	+121
Sävja	591	+53	+62	+80	+77	+97	+115
Hågaån							
Lurbo	584	+51	+55	+71	+71	+85	+98
Sävaån							
Ransta	586	+51	+54	+69	+70	+82	+94
Örsundaån							
Härnevi	588	+51	+53	+68	+69	+80	+92

Mean annual air temperature for the reference period 1961-1990 was higher in Ekoln than Galten with 5.3-5.8 °C and 3.8-5.0 °C, respectively. Increases projected by the future climate scenarios were very similar for all catchments, at most differing 0.2 °C between catchments within the same period and RCP scenario. Until 2040-2069, the projected increase in annual mean temperature were 2.7-2.8 °C under RCP2.6, 3.0 °C under RCP6.0 and 3.8-3.9 °C under RCP8.5. Until 2070-2099, the projected

increase in mean annual temperature was 2.4-2.6 °C under RCP2.6, 4.0-4.1 °C under RCP6.0 and 5.7-5.8 °C under RCP8.5. The increase was evenly distributed over the whole year, and no difference could be observed between catchments. Therefore, air temperature anomalies of Dalkarlshyttan were shown to represent the overall behaviour (figure 11A).

Simulated mean annual soil temperatures during the reference period were 5.4-6.2 °C in Galten and 6.5-6.7 °C in Ekoln. Soil temperature increases were rather similar across all catchments, with a slightly higher increase in the Ekoln catchments. Until 2040-2069, simulated mean annual soil temperature increase was 1.9-2.1 °C under RCP2.6, 2.1-2.4 °C under RCP6.0 and 2.7-3.2 °C under RCP8.5. Until 2070-2099, the simulated mean annual soil temperature increase was 1.7-2.0 °C under RCP2.6, 2.9-3.3 °C under RCP6.0 and 4.5-4.9 °C under RCP8.5. As for air temperature, the impact on simulated monthly soil temperature annomalies showed the same general pattern in all catchments (figure 11B). Under all RCP scenarios and time periods, the largest median monthly soil temperature increase occured in May and the smallest in January to March. From May until the winter, soil temperatures anomalies were gradually decreasing.

The number of simulated growing days increased for both future periods and all RCP scenarios (table 14). During the reference period, the number of simulated growing days were 194-207 in Galten and 210-213 in Ekoln. There was a gradual increase in number of growing days from west to east. The growing period was extended both towards the spring and autumn. Under RCP2.6 the number of growing days increased until 2040-2069, but then slightly decreased during 2070-2099 for all catchments. Under RCP6.0 and 8.5 the number of growing days increased between the two future periods. The increase in growing days was higher in the study catchments draining into Ekoln, which already had a longer growing season during the simulated reference period.

GWLF simulates evapotranspiration which is regulated by potential evapotranspiration, growing season, and available soil moisture in the unsaturated zone. During the reference period, evapotranspiration in Galten was 408-461 mm $year^{-1}$ and in Ekoln 396-445 mm $year^{-1}$ (table 15). All 13 catchments showed similar evapotranspiration behaviour over the coming century, both annually and monthly. Therefore, only the evapotranspiration for Dalkarlshyttan is shown (figure 12). All three RCP scenarios showed a higher annual evapotranspiration compared to the reference period although they all went up and down during the coming century. Under RCP2.6, evapotranspiration was slightly lower in 2070-2099 compared to 2040-2069 in the Galten catchments but slightly higher in the Ekoln catchments. All catchments had a higher evapotranspiration in 2070-2099 compared to 2040-2069 under both RCP6.0 and 8.5 2070-2099.

The largest simulated monthly change in median evapotranspiration was seen in the spring months, March, April and May where all three scenarios and both periods showed an increase. The increase was larger in the higher RCP scenarios. Under RCP2.6, August showed a higher median increase than under RCP6.0 and 8.5. During the summer months, June, July and August, evapotranspiration showed a larger spread around the median value, meaning that there would be an increase in some years and decrease in

others. The autumn and winter months showed only a slight increase in evapotranspiration, with a smaller spread, and similar for all three RCP scenarios as well as both periods.

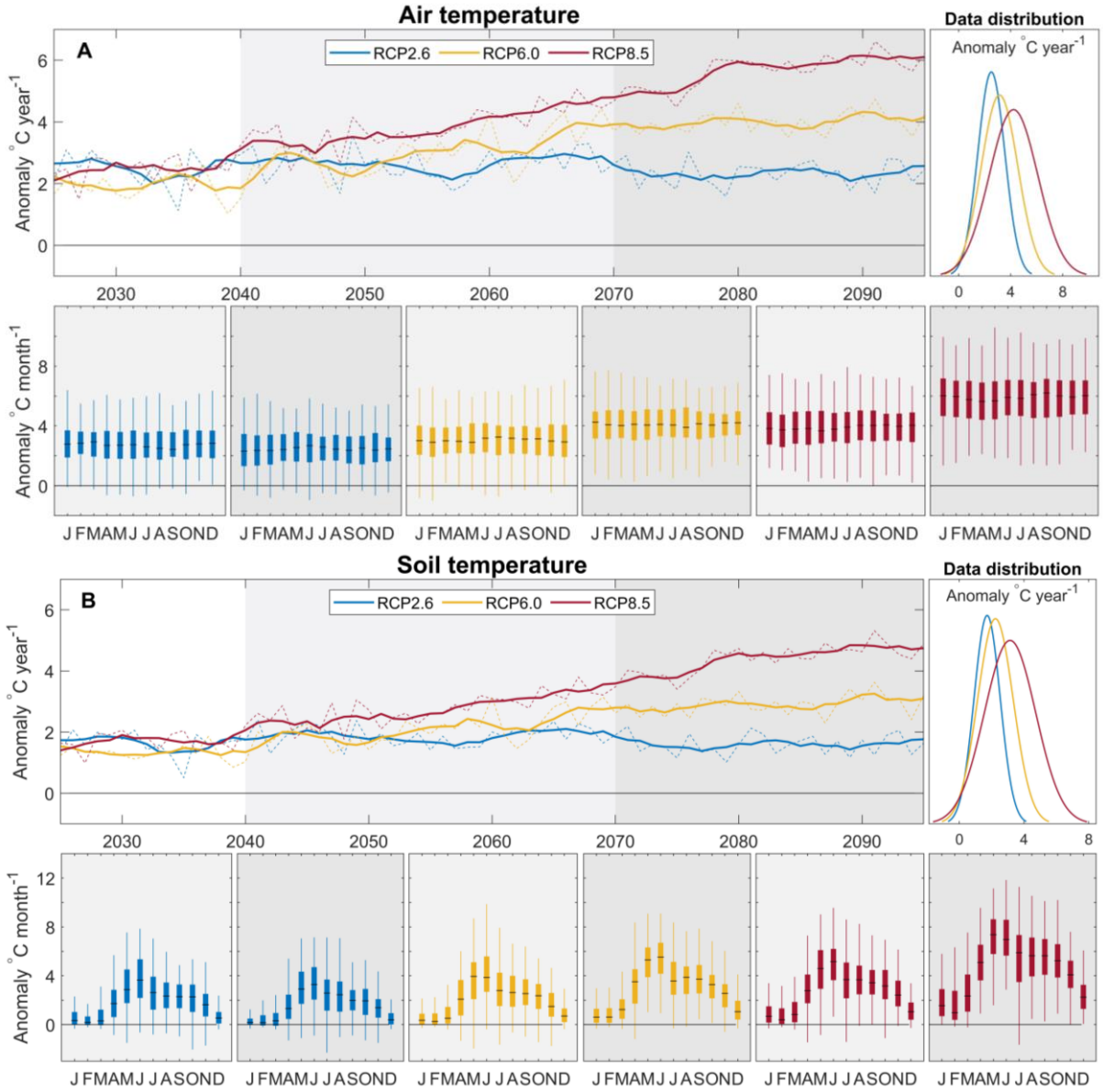

Figure 11 (A) Air and **(B)** soil temperature anomalies for Dalkarlshyttan. For both air and soil temperature: Top left: mean annual (dashed line) and 5-year moving average (solid line) for the three RCP scenarios compared to the reference period 1961-1990. Top right: Annual data distribution for the whole period, including all four GCM's. Bottom: Mean monthly anomaly for the period 2040-2069 (light grey) and 2070-2099 (darker grey), including the whole 30 year-periods and all four GCM's.

Table 14 Mean annual growing days during a year in the period 1961-1990 and the mean change for the three RCP2.6, 6.0 and 8.5 in the periods 2040-2069 and 2070-2099. All four GCM's are used to calculate the mean.

Growing days	Reference	2040-2069			2070-2099		
	1961-1990	RCP2.6	RCP6.0	RCP8.5	RCP2.6	RCP6.0	RCP8.5
Arbogaån							
Dalkarlshyttan	194	+30	+35	+48	+26	+49	+83
Kåfalla	197	+32	+38	+51	+28	+53	+86
Hammarby	196	+31	+37	+51	+26	+51	+85
Kringlan	195	+31	+36	+49	+26	+50	+83
Fellingsbro	202	+34	+42	+56	+32	+59	+92
Hedströmmen							
Dömsta	200	+34	+41	+55	+30	+57	+90
Köpingsån							
Odensvibron	207	+41	+47	+62	+36	+66	+98
Fyrisån							
Ulva Kvarndamm	211	+42	+49	+66	+36	+69	+101
Vattholma	212	+42	+49	+66	+37	+70	+101
Sävja	213	+42	+48	+65	+37	+70	+101
Hågaån							
Lurbo	212	+41	+48	+64	+36	+68	+99
Sävaån							
Ransta	212	+41	+48	+65	+36	+68	+99
Örsundaån							
Härnevi	210	+42	+49	+65	+36	+68	+99

Table 15 Mean annual evapotranspiration in mm year^{-1} for the reference period 1961-1990 and mean annual change in mm year^{-1} for the three RCP2.6, 6.0 and 8.5 in the periods 2040-2069 and 2070-2099. All four GCM's are used to calculate the mean.

Evapotranspiration (mm year^{-1}*)*	1961-1990	2040-2069			2070-2099		
	Reference	RCP 2.6	RCP 6.0	RCP 8.5	RCP 2.6	RCP 6.0	RCP 8.5
Arbogaån							
Dalkarlshyttan	408	+48	+47	+57	+45	+67	+88
Kåfalla	450	+60	+61	+76	+57	+89	+115
Hammarby	455	+53	+54	+65	+48	+73	+101
Kringlan	437	+46	+48	+56	+42	+64	+89
Fellingsbro	443	+56	+53	+67	+52	+77	+98
Hedströmmen							
Dömsta	450	+57	+56	+70	+53	+82	+104
Köpingsån							
Odensvibron	461	+56	+54	+68	+54	+78	+100
Fyrisån							
Ulva Kvarndamm	396	+49	+46	+59	+51	+72	+86
Vattholma	422	+54	+52	+67	+56	+81	+97
Sävja	416	+51	+50	+66	+56	+79	+94
Hågaån							
Lurbo	432	+50	+47	+61	+53	+72	+89
Sävaån							
Ransta	445	+50	+48	+59	+52	+70	+86
Örsundaån							
Härnevi	445	+51	+49	+60	+52	+71	+89

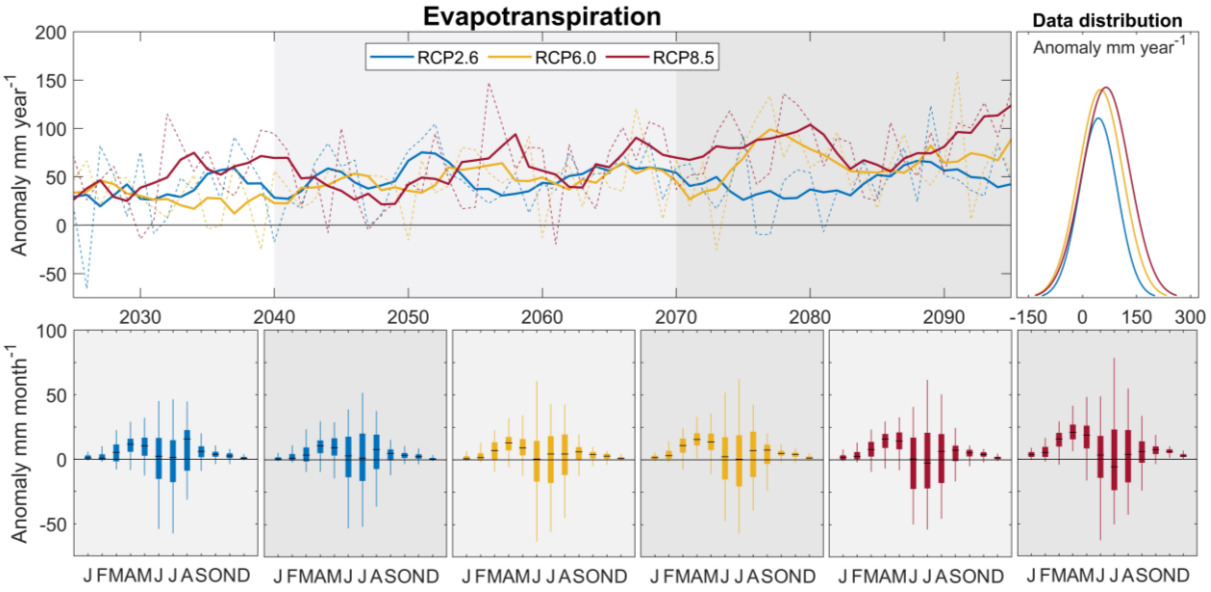

Figure 12 Evapotranspiration anomalies for Dalkarlshyttan, which was chosen to represent all the study catchments. Top left: mean annual (dashed line) and 5-year moving average (solid line) for the three RCP scenarios compared to the reference period 1961-1990. Top right: Annual data distribution for the whole period, including all four GCM's. Bottom: Mean monthly anomaly for the period 2040-2069 (light grey) and 2070-2099 (darker grey), including the whole 30 year-periods and all four GCM's.

3.4 Hydrological response to climate change

Simulated streamflow for the reference period was 281-401 mm year^{-1} in the Galten catchments and 208-315 mm year^{-1} in the Ekoln catchments. All catchments showed a similar mean annual response, with streamflow for all three future climate scenarios alternating between having the largest increase or decrease during the future simulations (figure 13). Despite this variability when compared to the reference period, all RCP scenarios showed an average increase in streamflow in the periods 2040-2069 to 2070-2099, although there was no distinct difference across all catchments between the three RCP scenarios (table 16). Under RCP2.6 and 6.0, simulated annual streamflow increased for all catchments between the two future periods, although the increase was more pronounced for RCP2.6. Under RCP8.5 simulated streamflow decreased slightly between the two periods for all Galten catchments and increased slightly for all Ekoln catchments except Härnevi, where it remained unchanged (table 16).

Whereas simulated annual streamflow was not showing a clear trend, seasonal patterns were clearly shown (figure 13). Streamflow simulations showed an increase in future median winter streamflow during December, January, February, and March for all catchments and all three RCP scenarios, although to a varying extent and with increased magnitude for the higher RCP scenarios. All catchments showed a large decrease in median streamflow during April to June, and often a smaller decrease during the remainder of the summer and autumn. December to March displayed the largest variation and ranged from an increase of almost 75 mm year^{-1} to a decrease of 25 mm year^{-1}.

Two catchments, Dalkarlshyttan and Vattholma, are shown to represent simulated streamflow response based on monthly changes for Galten and Ekoln, respectively. Despite being in Galten,

streamflow response in Odensvibron was behaving more like the Ekoln catchments, and the behaviour of Kåfalla and Fellingsbro fell somewhere in between. The Galten catchments showed a more pronounced increase in winter streamflow and largest decrease in May streamflow. They had the smallest streamflow change in July to September. Simulated streamflow in the Ekoln catchments decreased most in April and showed no change in median streamflow as well as a very small variation in June to November.

Simulated baseflow displayed very similar changes in annual and seasonal flow in the future climate scenarios as simulated streamflow, although with a lower total magnitude (figure 14A). The exception was in April where there was no change in median simulated baseflow, but a decrease in median streamflow. Runoff response was, however, more different from baseflow and streamflow response (figure 14B). The Galten catchments showed a large runoff decrease in April and May, and a slight increase during January and Februray, except for Fellingsbro where baseflow decreased every month. The Ekoln catchments and Odensvibron showed a median decrease during all months, also with the largest decrease in April but with a smaller change from December to April. Summer and fall months showed the smallest runoff change in all catchments. Contribution of runoff and baseflow to total streamflow in the reference period ranged between 12-18% and 82-88 % respectively in Galten and 11-28 % and 72-89 % in Ekoln. Relative contribution of baseflow increased slightly in the future scenarios, with a larger baseflow increase in the Ekoln catchments.

Table 16 Mean annual streamflow in mm year^{-1} for the reference period 1961-1990 and mean annual change in mm year^{-1} for the three RCP2.6, 6.0 and 8.5 in the periods 2040-2069 and 2070-2099. All four GCM's are used to calculate the mean.

Streamflow	1961-1990	2040-2069			2070-2099		
(mm year^{-1}*)*	Reference	RCP 2.6	RCP 6.0	RCP 8.5	RCP 2.6	RCP 6.0	RCP 8.5
Arbogaån							
Dalkarlshyttan	359	+17	+12	+25	+28	+23	+23
Kåfalla	401	+20	+12	+25	+39	+26	+21
Hammarby	392	+10	+6	+19	+23	+14	+13
Kringlan	380	+13	+9	+22	+23	+17	+18
Fellingsbro	295	+13	+10	+21	+32	+24	+20
Hedströmmen							
Dömsta	339	+17	+13	+24	+36	+27	+23
Köpingsån							
Odensvibron	281	+11	+11	+18	+34	+25	+16
Fyrisån							
Ulva Kvarndamm	208	+10	+14	+18	+26	+22	+25
Vattholma	247	+11	+16	+20	+31	+25	+29
Sävja	214	+6	+16	+18	+26	+25	+28
Hågaån							
Lurbo	315	+15	+23	+29	+37	+36	+36
Sävaån							
Ransta	260	+12	+16	+24	+31	+28	+26
Örsundaån							
Härnevi	261	+11	+14	+21	+31	+26	+21

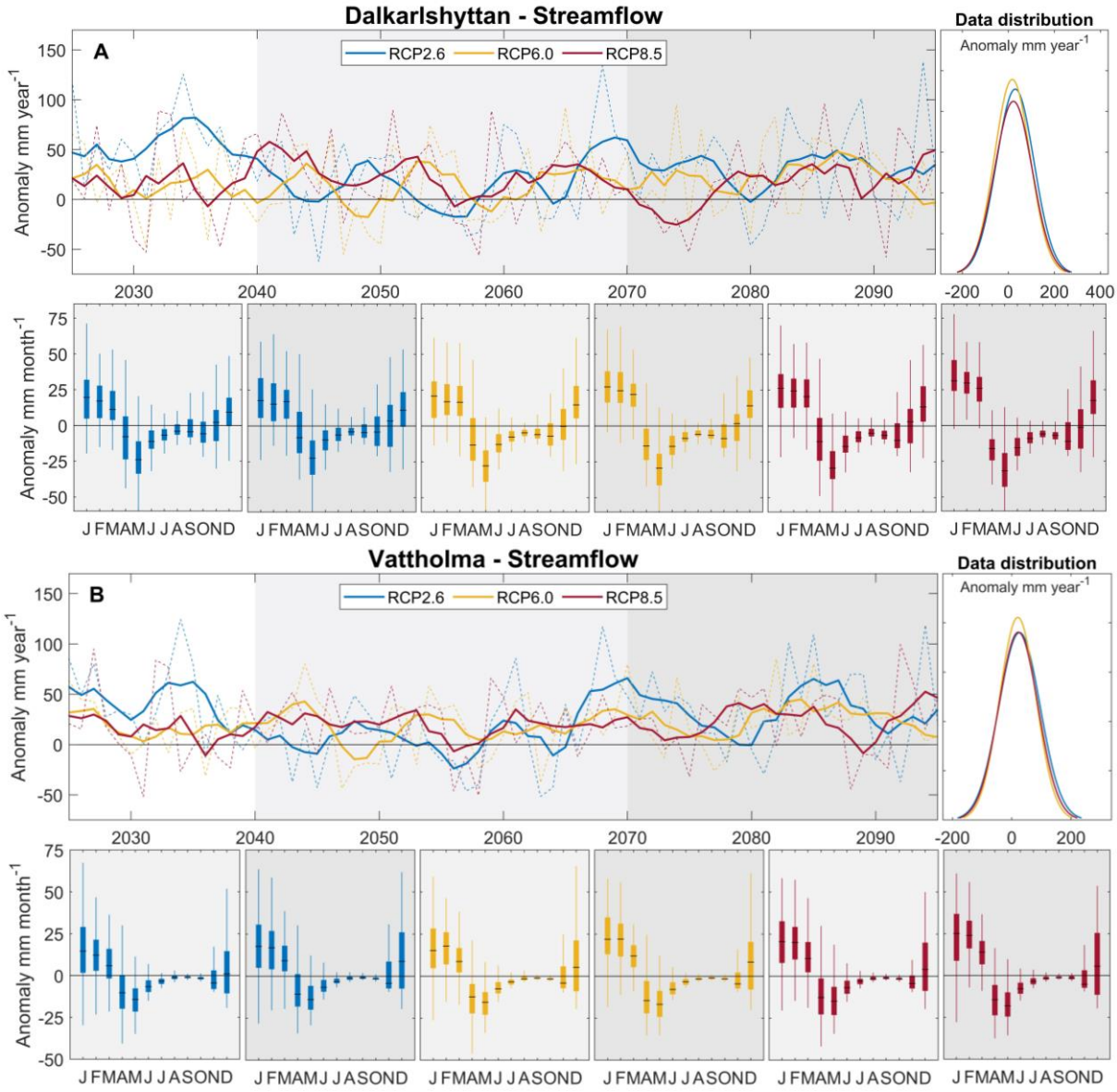

Figure 13 Streamflow anomalies for **(A)** Dalkarlshyttan and **(B)** Vattholma. For each cathment; top left: mean annual (dashed line) and 5-year moving average (solid line) for the three RCP scenarios compared to the reference period 1961-1990. Top right: Annual data distribution for the whole period, including all four GCM's. Bottom: Mean monthly anomaly for the period 2040-2069 (light grey) and 2070-2099 (darker grey), including the whole 30 year-periods and all four GCM's.

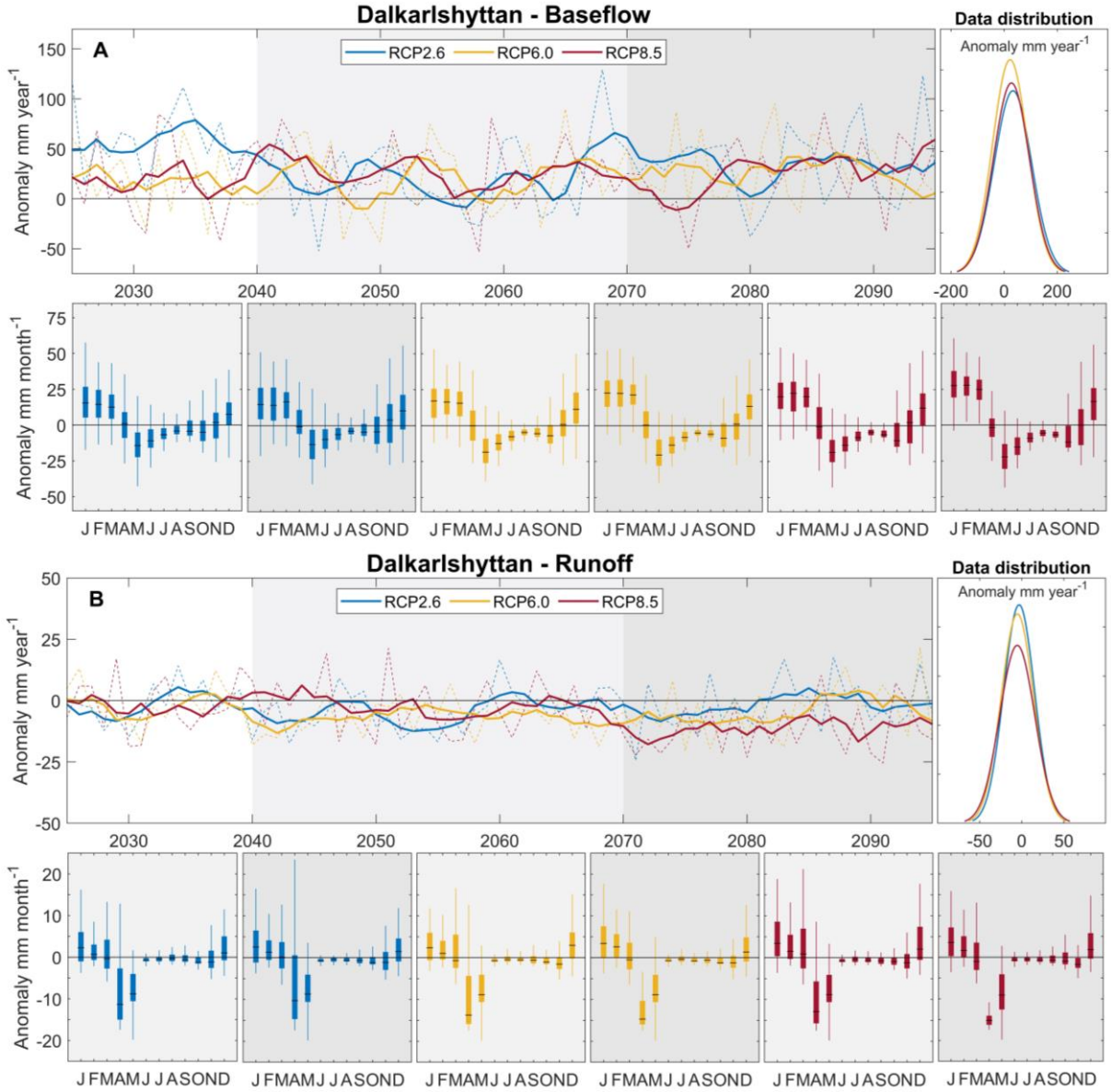

Figure 14 (A) Baseflow and **(B)** runoff responses for Dalkarlshyttan. For each response; top left: mean annual (dashed line) and 5-year moving average (solid line) for the three RCP scenarios compared to the reference period 1961-1990. Top right: Annual data distribution for the whole period, including all four GCM's. Bottom: Mean monthly anomaly for the period 2040-2069 (light grey) and 2070-2099 (darker grey), including the whole 30 year-periods and all four GCM's.

The simulated water content of the unsaturated zone decreased over all RCP scenarios and catchments and continued to decrease over the whole period. The median monthly decrease was largest during the growing period and the range was quite large. The only month that showed an increase in median water content of the unsaturated zone was November, which increased under most scenarios and time periods. The saturated zone showed the same behaviour as total streamflow and baseflow, both in annual and monthly water content. Water content of the deep saturated zone decreased during June to October for all future scenarios and catchments and the range of decrease was fairly similar for all three RCP scenarios, although the median decrease was generally greater with higher RCP scenarios. Over the whole period, there was a slight annual decrease of water content in the deep saturated zone.

3.5 DOC response to climate change

Simulated DOC concentrations for the reference period ranged from 8.5-13.8 mg l^{-1} in Galten and 11.5-15.5 mg L^{-1} in Ekoln (table 17). Concentrations increased in all catchments and scenarios compared to the reference period. The highest concentration increase was seen under RCP8.5 in both future periods. Under RCP2.6, DOC concentrations in Odensvibron and all Ekoln catchments, except for Sävja, decreased from 2040-2069 to 2070-2099. In the Galten catchments, concentrations increased under RCP2.6, although less than the increases seen under RCP6.0 and 8.5. Median DOC concentrations increased during the whole year, but the increase was larger from December to March (figure 15). The catchments that showed a decrease under RCP2.6 in 2070-2099 also showed a less pronounced winter increase. Concentration increases were generally lowest in late summer to fall.

Mean annual DOC loads for the reference period were 3.5-4.2 tC km^2 $year^{-1}$ in Galten and 2.6-4.2 tC km^2 $year^{-1}$ in Ekoln. As for concentrations, DOC loads showed an increase in all future scenarios compared to the reference period. The catchments that showed a decrease in concentrations from 2040-2069 to 2070-2099 under RCP2.6 also showed a decrease in loads during this period. The largest increase in loads was seen under RCP8.5. There was a strong seasonal response in changes in DOC loads, with a larger increase in the winter months and almost no change in DOC loads during the summer and fall months (figure 16).

Regression analyses were done on land cover and annual DOC loads and concentrations (figure 17). DOC concentrations in the reference period decreased with larger areal percentage of coniferous forest (R^2=0.52, p=0.003) and increased with increased areal percentage of agriculture (R^2 =0.33, p=0.02). Plotting these did however show two clear groups of data points (figure 17A). Therefore, these were split and analysed separately. Now, only the group with an agricultural area of more than 7% showed a significant correlation with DOC concentrations, where concentrations decreased with higher percentage of agriculture (R^2=0.43, p=0.05; figure 17B). These were the Ekoln catchments as well as Odensvibron and Fellingsbro. The regression analyses also showed that the increase in DOC loads were higher in catchments with a higher percentage of coniferous forest in 2040-2069 for RCP2.6 (R^2=0.26, p=0.05), RCP6.0 (R^2=0.36, p=0.02), and RCP8.5 (R^2=0.35, p=0.02) as well as in 2070-2099 for RCP6.0 (R^2=0.38, p=0.01) and RCP8.5 (R^2=0.47, p=0.006) (figure 17C). As with concentrations during the reference period, DOC loads decreased with areal extent of agriculture under RCP8.5 in 2070-2099 (R^2=0.28, p=0.04) (figure 17C).

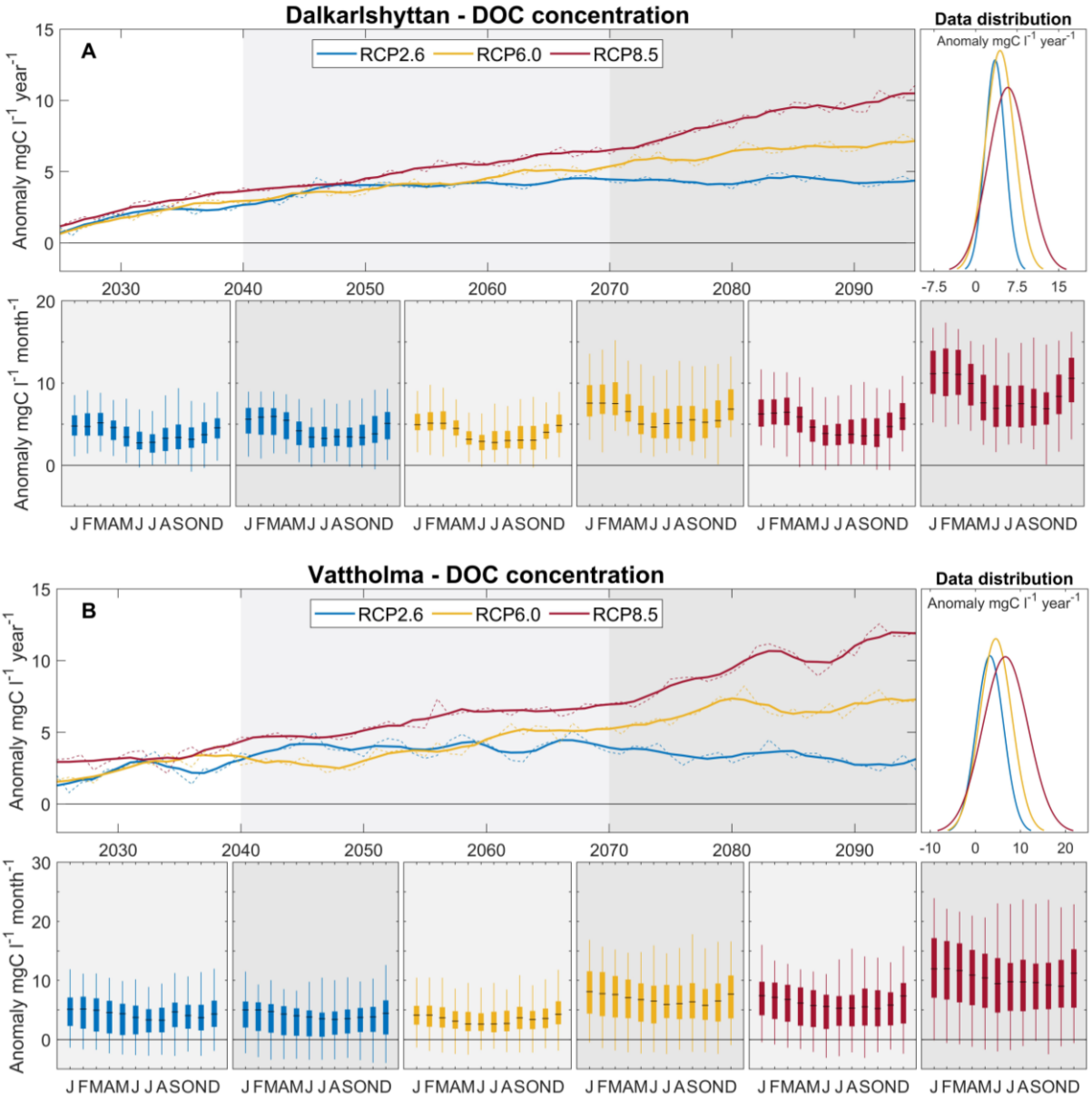

Figure 15 DOC concentration (mgC l^{-1}) anomalies for **(A)** Dalkarlshyttan and **(B)** Vattholma. For each cathment; top left: mean annual (dashed line) and 5-year moving average (solid line) for the three RCP scenarios compared to the reference period 1961-1990. Top right: Annual data distribution for the whole period, including all four GCM's. Bottom: Mean monthly anomaly for the period 2040-2069 (light grey) and 2070-2099 (darker grey), including the whole 30 year-periods and all four GCM's.

Table 17 Simulated mean annual DOC concentrations (mg L^{-1}) in streamflow for the reference period (1961-1990) and mean annual changes in the two future periods for three RCP-scenarios for each catchment.

mgC l^{-1}	1961-1990	2040-2069			2070-2099		
	Reference	RCP2.6	RCP6.0	RCP8.5	RCP2.6	RCP6.0	RCP8.5
Arbogaån							
Dalkarlshyttan	9.7	+3.9	+4.1	+5.1	+4.4	+6.5	+9.0
Kåfalla	8.5	+4.4	+4.5	+5.4	+5.6	+7.2	+9.3
Hammarby	8.5	+2.5	+2.9	+3.7	+2.7	+4.8	+7.2
Kringlan	10.0	+3.9	+4.2	+5.2	+4.3	+6.7	+9.5
Fellingsbro	12.0	+4.4	+4.6	+5.8	+4.6	+7.1	+10.1
Hedströmmen							
Dömsta	9.2	+5.5	+5.5	+6.5	+7.1	+9.0	+11.3
Köpingsån							
Odensvibron	13.8	+3.3	+3.1	+4.8	+2.5	+5.5	+9.4
Fyrisån							
Ulva Kvarndamm	11.5	+2.8	+2.7	+4.0	+2.3	+4.8	+7.1
Vattholma	15.5	+4.0	+3.8	+5.7	+3.3	+6.7	+9.9
Sävja	13.4	+7.8	+7.4	+9.1	+9.6	+11.6	+14.7
Hågaån							
Lurbo	11.6	+2.9	+2.8	+4.2	+2.3	+4.9	+7.7
Sävaån							
Ransta	11.5	+2.5	+2.5	+3.8	+2.2	+4.6	+7.2
Örsundaån							
Härnevi	12.3	+3.3	+3.1	+4.6	+3.0	+5.4	+8.4

Table 18 Mean annual DOC loads in t km^{-2} for the reference period (1961-1990) and mean annual changes in the two future periods for three RCP-scenarios for each catchment.

tC km^{-2} yr^{-1}	1961-1990	2040-2069			2070-2099		
	Reference	RCP2.6	RCP6.0	RCP8.5	RCP2.6	RCP6.0	RCP8.5
Arbogaån							
Dalkarlshyttan	3.8	+1.8	+1.8	+2.3	+2.0	+2.8	+3.9
Kåfalla	3.7	+2.2	+2.2	+2.7	+2.7	+3.4	+4.4
Hammarby	3.4	+1.3	+1.4	+1.8	+1.3	+2.1	+3.3
Kringlan	4.1	+1.9	+2.0	+2.6	+2.1	+3.0	+4.5
Fellingsbro	3.9	+1.6	+1.7	+2.3	+1.8	+2.6	+3.7
Hedströmmen							
Dömsta	3.5	+2.3	+2.2	+2.8	+3.0	+3.6	+4.6
Köpingsån							
Odensvibron	4.2	+1.2	+1.3	+1.8	+1.1	+2.0	+3.2
Fyrisån							
Ulva Kvarndamm	2.6	+0.8	+0.8	+1.1	+0.8	+1.2	+1.9
Vattholma	4.2	+1.3	+1.2	+1.8	+1.2	+1.9	+3.0
Sävja	3.8	+2.3	+2.3	+2.8	+3.0	+3.4	+4.5
Hågaån							
Lurbo	4.2	+1.4	+1.5	+2.1	+1.3	+2.2	+3.6
Sävaån							
Ransta	3.4	+1.0	+1.0	+1.4	+0.9	+1.5	+2.5
Örsundaån							
Härnevi	3.5	+1.2	+1.2	+1.7	+1.2	+1.8	+2.8

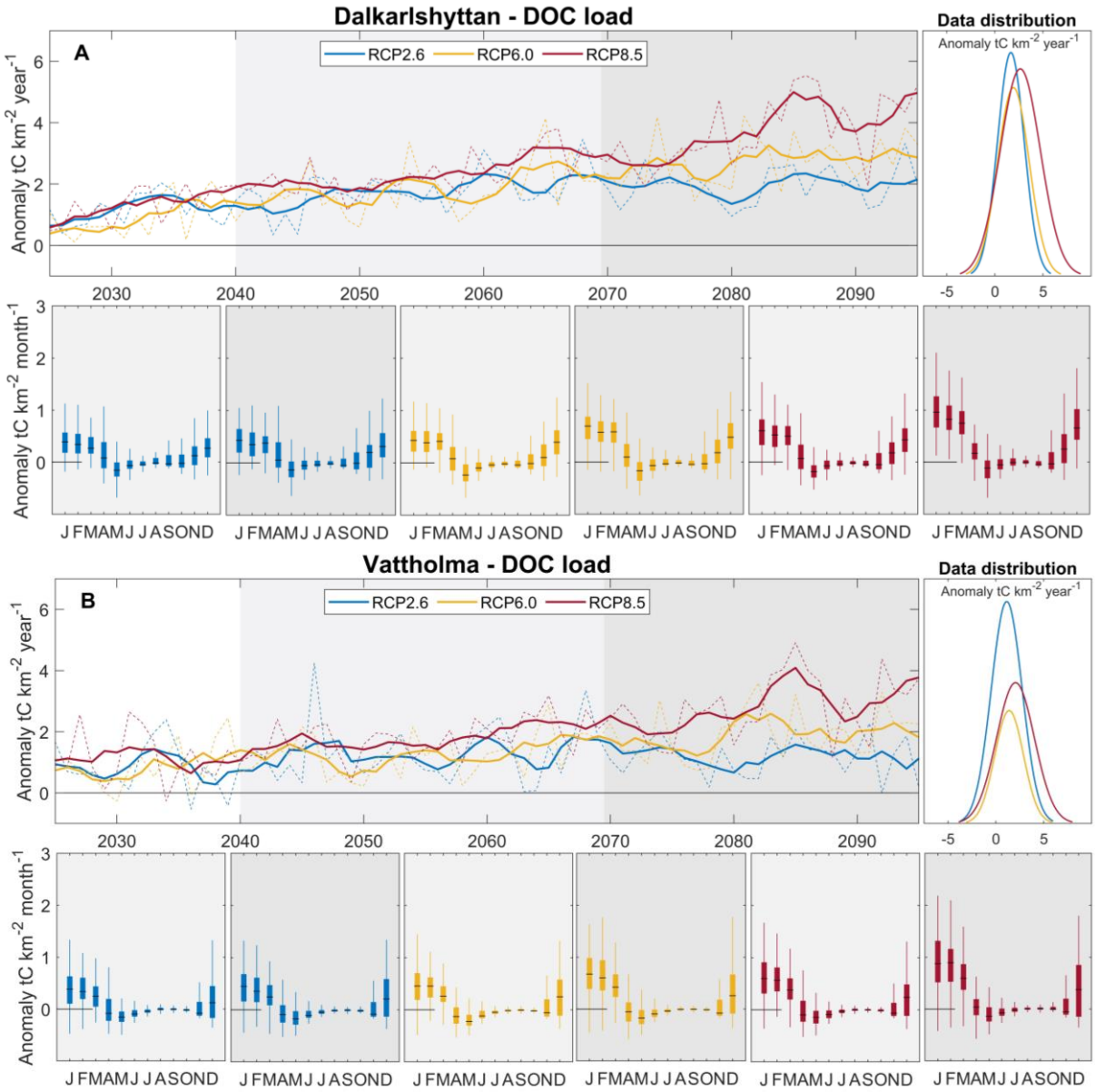

Figure 16 DOC load (tC km^{-2}) anomalies for **(A)** Dalkarlshyttan and **(B)** Vattholma. For each cathment; top left: mean annual (dashed line) and 5-year moving average (solid line) for the three RCP scenarios compared to the reference period 1961-1990. Top right: Annual data distribution for the whole period, including all four GCM's. Bottom: Mean monthly anomaly for the period 2040-2069 (light grey) and 2070-2099 (darker grey), including the whole 30 year-periods and all four GCM's.

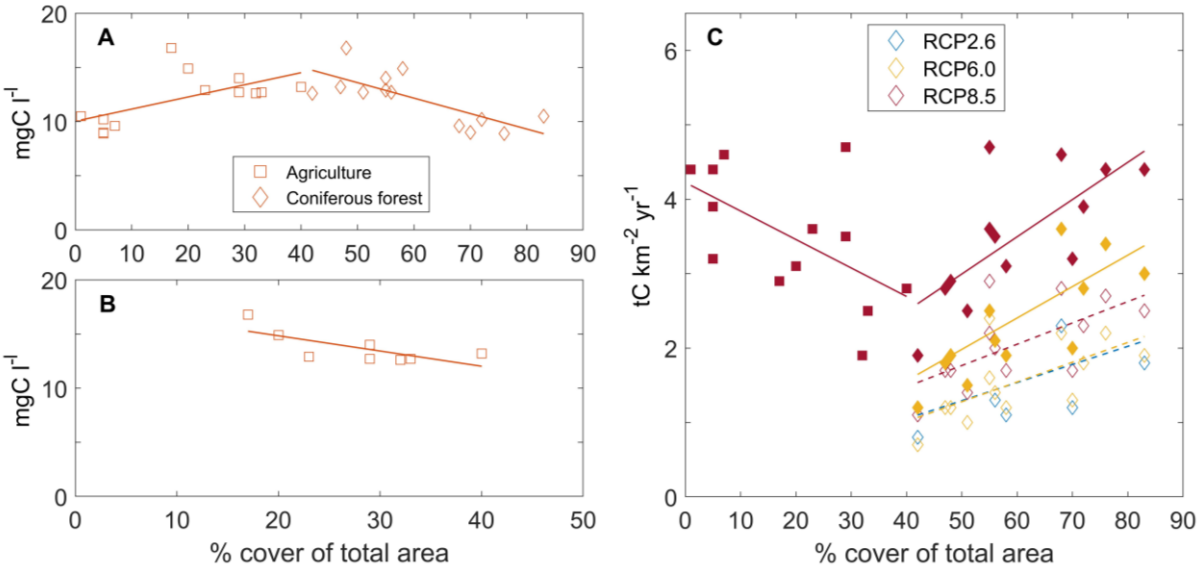

Figure 17 Correlation between land cover and **(A&B)** DOC concentrations and **(C)** DOC loads. Diamonds represent coniferous forest, squares agriculture and circles peat bogs. Colours represent each scenario; orange for reference period; blue for RCP2.6, yellow for RCP6.0 and red for RCP8.5. Unfilled blue, yellow and red symbols represent the period 2040-2069 and filled 2070-2099. Figure A and C show correlations with all catchments, and figure B show only the catchments with agricultural area >7%.

3.6 DOC loads to Galten and Ekoln

Total DOC loads simulated in the examined catchments were summed for both Galten and Ekoln, covering an area of 3854 and 2317 km^2, respectively. Simulated mean annual loads from these catchments during the reference period were 14 020 tC to Galten and 7 560 tC to Ekoln. Total mean annual loads to both basins were larger for all scenarios and time periods compared to the reference period and increased from 2040-2069 to 2070-2099 (table 19). Highest increase in load was seen under RCP8.5 in 2070-2099, when DOC loading more than doubled in Galten and nearly doubled in Ekoln.

The simulated median monthly DOC loads increased during winter to both basins under all RCP scenarios and both future periods (figure 18). In Galten, the increase was seen from November to April and in Ekoln from December to March. Median monthly DOC loads to Galten were slightly decreasing in May, June, September, and October. In Ekoln, they decreased in April, May, and November. During the period with decreasing loads, they were also similar between the three RCP scenarios. During the winter, however, there was a larger difference between the scenarios, with larger loads for higher RCP scenarios. Under RCP2.6 there was only a small difference between the two future periods, but RCP6.0 and RCP8.5 increased more from 2040-2060 to 2070-2099.

Table 19 Total mean annual DOC loads from the examined catchments in Galten and Ekoln for the reference period (1961-1990) and mean annual changes in the two future periods for three RCP-scenarios.

tC yr^{-1}	1961-1990	2040-2069			2070-2099		
	Reference	RCP2.6	RCP6.0	RCP8.5	RCP2.6	RCP6.0	RCP8.5
Galten	14020	+6941	+7059	+9030	+8161	+11026	+15315
Ekoln	7560	+3213	+3166	+4169	+3626	+4821	+6931

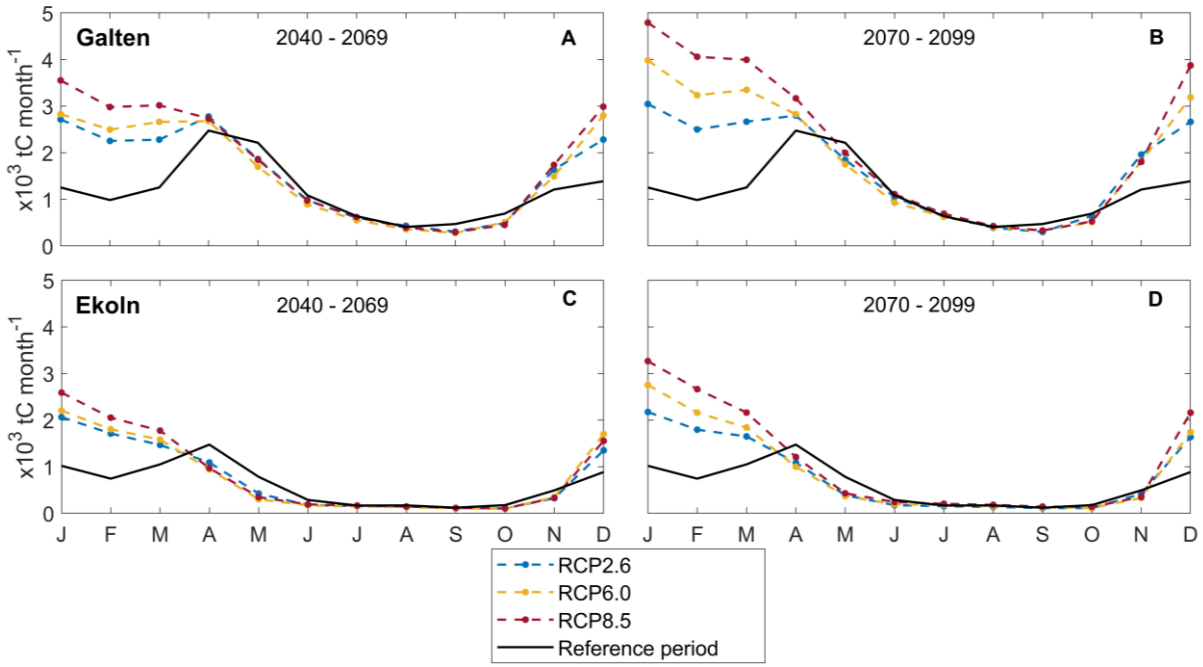

Figure 18 Total median monthly DOC loads from the examined catchments into **(A & B)** Galten and **(C & D)** Ekoln during the reference period 1961-1990 (black line) and RCP2.6 (dashed blue line), RCP6.0 (dashed yellow line) and RCP8.5 (dashed red line) for the two future periods 2040-2069 and 2070-2099.

4 Discussion

4.1 Model performance

Hydrological model performance, indicated by NSE and R^2 values, showed a similar performance as was obtained in the CLIME-project, although with a lower runoff performance (Schneiderman et al. 2009). Streamflow NSE is in some Galten catchments slightly lower than that of Moore et al. (2008), although these were reported as monthly streamflow and using shorter periods, likely resulting in higher NSE performance. Comparing the performance of the GWLF-hydrology model in this study to model studies using the HBV-model, the fit found here are slightly lower for some catchments, but other perform similar. Seibert (1999) and Ledesma et al. (2012) also simulated streamflow in catchments draining into the Ekoln basin and found NSE of 0.70-0.88, compared to streamflow NSE in this study of 0.58-0.76. The studies of Seibert (1999) and Ledesma et al. (2012) also used shorter time periods, which might in some cases result in a higher model fit.

Performance of simulated DOC concentrations are generally lower than that in the CLIME-project although some R^2 values in this study are higher (Naden et al. 2009). The range of performance seen in this study is reasonable as thirteen catchments were modelled, which is more than in most studies. Modelling of DOC with the INCA-C model in Sweden by Ledesma et al. (2012) and Futter et al. (2011) gave NSE and R^2 values of 0.39-0.52 and 0.39-0.53, respectively. In Canada, Futter et al. (2007) showed a DOC model performance with NSE of 0.45-0.66 and Oni et al. (2011) R^2 of 0.12-0.53. Considering this, the performance of the GWLF-DOC model in this study should be considered rather successful, even though the performance for some catchments fell well below these studies. As in this study, studies of simulated DOC with the INCA-C model also report difficulties in capturing peak DOC concentrations. In fact, the peak concentration seen in Vattholma in 2009 is better captured in this study than the corresponding peak in Fyrisån by INCA-C in the study by Ledesma et al. (2012). The ability of the GWLF-DOC model to replicate the upward trends seen in Fellingsbro and Vattholma during the last three decades show great promise in its ability to simulated DOC under future climate.

The calibration method in this study differs from some others that use Monte Carlo iterations until the best possible R^2 or NSE is achieved (i.e Ledesma et al. 2012). Whereas here, parameters are calibrated against relationships between simulated and either direct measurements or processed measured data. There is reason to argue that this calibration method is more robust and more likely to produce catchment specific parameters. Consequently, it reduces the risk of obtaining a random parameter set that happens to produce a good result.

Both hydrological and DOC parameters are influenced by catchments characteristics. Together with the sensitivity analysis, this indicates that the parameter values are not being optimised at random values but are reflecting the catchment characteristics. The hydrological model performed better than the DOC model, with higher goodness-of-fit values. Only two soil types, bedrock and glaciofluvial deposits, were found to impact the hydrology model performance of runoff and baseflow. No soil types or land covers

impacted the model's performance in simulating streamflow. This means that the hydrology model can be applied on a wide range of soils and land covers. Performance of simulated DOC concentrations was impacted by several land covers and soil types, with increasing percentage of agriculture and clay-silt cover decreasing the performance of simulated DOC concentrations. Further attention should be paid towards this in the future.

This study shows that the model is able to successfully simulate DOC loads in the current climate across the examined catchments, despite the fact that the model was not originally developed for forested mineral soils. However, given that the GWLF-DOC model is very simple and does not explicitly include many processes that are known to impact DOC export in boreal regions, uncertainties of how these will impact DOC export in the future is important to acknowledge. As chemical soil and in-stream processes are not explicitly included in the model, changes in these and the impact on DOC might not be captured in the current model processes. The only processes currently being replicated by the model is the effects of soil temperature and soil moisture on DOC decomposition.

4.2 Impacts of climate change

Based on the climate scenarios, simulated future hydrology and DOC to lake Mälaren will be characterized by lower flows in spring and summer, and higher in winter (figure 13). This will mainly be due to changes in temperature as precipitation is not projected to change much during the spring months, that also show the largest streamflow decrease (figure 10). Instead, the higher simulated evapotranspiration reduces soil moisture and streamflow. The increased annual evapotranspiration counteracts the increasing annual precipitation, resulting in a lower increase in simulated annual streamflow than would otherwise be occurring. In addition, higher temperatures will result in more precipitation falling as rain instead of snow during winter, a reduced snowpack accumulation and a greater winter snowmelt. Less snow will therefore melt during spring, thus reducing the spring flood. The temperature dependent impacts are larger later in the century for RCP6.0 and RCP8.5 but for RCP2.6 there is a smaller or even decrease in impacts in 2070-2099 compared to 2040-2069, as this is the scenario with the strongest mitigation (Frieler et al. 2017).

Air temperature will increase in all months and result in a longer growing season and warmer soil temperatures, most pronounced during spring and summer. Higher soil temperatures will lead to higher decomposition rates of organic material under both anaerobic and aerobic conditions. Warmer summers will result in higher evapotranspiration and reduced soil moisture which will increase aerobic decomposition until a certain point, after which decomposition rates decrease. Following decomposition, DOC remains stored in the soil until water transports it out of the soil column to streams and water bodies. In the future RCP scenarios, streamflow (including baseflow) decreases during spring and summer which means that less DOC can be transported to surface waters in this period even though decomposition is increasing. Instead, DOC can build up in the soils during this dryer period and then be washed out by the higher winter flows. According to the future scenarios, seasonal variations in DOC

loads show similar behaviour as streamflow which show the importance of stream discharge controlling the timing and magnitude of DOC loading (figure 13 & 16). However, loads do not decrease as much during spring and summer as streamflow. This could be explained by increasing DOC concentrations during all months, as well as a larger response in decreased runoff compared to baseflow which do not impact DOC transport to the same extent. DOC concentrations show a larger median increase during the winter months which could be explained by an increased infiltration into soils as increased winter air temperatures leads to less snow.

Simulated future DOC loads show a larger increase in catchments with a higher area of coniferous forest under all RCP scenarios in the future periods, although concentrations did not show the same pattern. Instead, DOC concentrations in the reference period were higher in the catchments with more agriculture and lower in the catchments with higher area of coniferous forest. The catchments with more agriculture also had the lowest streamflow (mm day^{-1}), highest number of growing days and highest soil temperatures during the reference period. There is no statistically significant correlation between increased future annual simulated streamflow and DOC loads in the future scenarios. Catchments with higher loads also show a lower value of the slow rate parameter, which is regulating DOC washout through subsurface and slow subsurface flow. Higher DOC export from coniferous forest is in line with studies that have shown that increased volume of spruce correlates with browner surface waters (Škerlep et al. 2019, Lindqvist 2020), despite area and volume of coniferous forest being kept constant in this study. If coniferous forest would further expand in the catchments, this might lead to a higher increase in DOC loadings. However, this would need to be further studied.

Modelling of DOC concentrations under future climate scenarios in Canada with the INCA-C model showed similar trends in annual DOC concentrations in the coming century (Oni et al. 2012). In addition, they also show a larger increase in concentrations during the winter months, as is seen in Galten and Ekoln. Responses are also similar to those found in the CLIME-project (Naden et al. 2009).

4.3 Data and process uncertainties

Even though both the hydrological and DOC model showed an overall good performance, it is important to acknowledge limitations that inevitably arise in all modelling studies. One key uncertainty is the future climate scenarios that are used as the basis of the future hydrological and DOC simulations (Hattermann et al. 2018). Precipitation and temperature were used from four different bias corrected GCM's to reduce these uncertainties. Despite this, future climate scenarios remain with large uncertainties and should not be interpreted as certain predictions of future climate.

Due to the low frequency data of DOC measurements, it is not certain that the DOC measurements used for model calibration have captured the true highs and lows that occur under all conditions, particularly during storm events. In some catchments, the simulated DOC concentrations show peaks and lows of DOC that are not shown in measurements. It is not possible to determine if these simulated concentrations in between measurements are representative of true behaviour or not.

The great importance of soil temperature on DOC production means that it is important to accurately determine this. Jungqvist et al. (2014) have shown that soil temperatures do not exceed 15°C during current climate across Sweden, which it does in this study. Despite this, the simple approach used here to simulate soil temperatures is successful on some sites both north and south of the study area, where measured summer soil temperatures did in fact exceed 15°C. These sites were however situated in open areas, and the effect of air temperature on soil temperature inside forests might be different. The study by Jungqvist et al. (2014) support the seasonal changes in soil temperatures found here, with largest increases in April to August, despite their soil temperature model being more complex. They simulated a maximum increase of 4.0°C in May in a northern Swedish catchment under climate scenario A1B, corresponding to RCP6.0, in 2061-2090. The mean soil temperature increases under RCP6.0 in 2070-2099 in this study was also found in May and reached a slightly higher level of 5.0°C. While this adds some confidence to the validity of the simulated soil temperatures, attention should be paid towards the possibility of soil temperatures being overestimated, given the importance of this parameter in controlling future trends in DOC concentration and loading. Despite this high simulated soil temperature increase, and the uncertainty as to whether this is realistic or not, the results show the great impact that higher temperatures could potentially have on the production of DOC.

According to future climate scenarios used in this study, summers will become dryer as temperatures and evapotranspiration increases. This leads to periods of lower soil moisture and thus an increased importance of aerobic compared to anaerobic decomposition. The soil moisture dependence on decomposition of organic matter is replicated in the decomposition equation (eq. 1). The aerobic decomposition coefficient was confined to a range based on literature due to low frequency data making it difficult to calibrate this parameter. Despite this, there is still a large uncertainty in this coefficient. Given estimated drier future climate the impact of this could be significant on the results. Other DOC parameters are also influencing DOC simulations, with a higher anaerobic decomposition coefficient generally yielding higher DOC concentrations and loads whereas higher values of slow rate and mineral adjustment coefficients gave lower DOC concentrations and loads. More work needs to be done, and more high frequency DOC measurements needs to be collected, to establish if these coefficients are properly representing catchment characteristics.

Many more factors affect production and export of DOC to freshwaters than those included in the current GWLF-DOC model. For example, the riparian zone has been identified as the most important part of the boreal forest in terms of DOC export (Ledesma et al. 2018). There is also breakdown of DOC occurring in surface waters and chemical processes in the soil, neither of these included in the model. Other, more complex DOC models such as the INCA-C model includes some of these processes. The INCA-C model also models litter fall, root breakdown and in-stream processes (Futter et al. 2007). In addition, the INCA-C model uses two soil boxes and models both DOC and DIC, dissolved inorganic carbon, as well as DIC loss to the atmosphere.

For a long time, browning in northern freshwaters was ascribed to a recovery from acid deposition. Effects of acid deposition, and recovery from it, are not included in the GWLF-DOC model. During some of the longer calibration periods this effect could also impact the DOC dynamics and thus impact the calibration results.

Despite not being as complex as some other existing models, the hydrological portion of the GWLF model has been found to perform equally well or even better compared to the SWAT model in hydrological discharge simulations, based on goodness of fit statistics (Niraula et al. 2013; Qi et al. 2017). Performance can also be influenced by the catchment that is being studied, as Qi et al. (2017) showed a better performance of the GWLF model in a humid catchment compared to an arid one. Benefits of the GWLF model include an easier set up and faster run time than many other models. Depending on the software used, it also allows for an easy adaptation of the model to the specific study interest and catchment characteristics. However, this also means that the models used in different studies can slightly differ.

In this study, calibration of the hydrological model was done with hydrograph separated baseflow and runoff based on Arnold et al. (1995) as was previously done in the CLIME-project. This is a rather crude method that treats all catchments the same. In reality, different hydrological responses will be observed between catchments. Other methods for hydrograph separation exist and might improve the hydrograph separation and thus model performance of the study catchments. Such methods include isotope and tracer hydrograph separation (Fischer et al. 2021). These require more data and will be more labor intense but should be considered for future studies.

4.4 Scaling up catchments

Two catchments that were examined in this study, Kringlan and Vattholma, are sub catchments within Hammarby and Ulva Kvarndamm. This allows an evaluation on how well catchments of this scale can be scaled up to represent a larger area. Kringlan constitutes 293 km^2 of the total 888 km^2 Hammarby catchment and Vattholma constitutes 261 km^2 of the larger 952 km^2 Ulva Kvarndamm catchment (table 5). Land cover is rather similar, but both of the smaller catchments have a larger area of coniferous forest and less agricultural land. The optimal hydrological parameters found for the smaller and larger catchments were not more similar than between other catchments. Optimized DOC parameters for Vattholma and Ulva Kvarndamm are very similar and those of Kringlan and Hammarby are rather similar, with the largest difference in the mineral soil adjustment factor.

Climate response was similar, although not identical between both Kringlan and Hammarby as well as Vattholma and Ulva Kvarndamm. The largest difference between the smaller and larger catchment can be seen for evapotranspiration, which is likely due to their differing land covers. Despite this, response in total streamflow was similar between the catchments. Seasonal streamflow response is near identical between the smaller and larger catchments.

DOC concentrations and loads for both the reference period and future scenarios are different between the smaller and larger catchments. In both cases, the smaller catchments show higher DOC concentrations and loads. The lower concentrations in the larger catchments can be attributed to both land cover and catchments sizes, as the retention time in streams and water bodies will be higher in a larger catchment. The increase in concentrations and loads are also higher in the smaller catchments, although the percentage increase in Vattholma and Ulva Kvarndamm is similar. In some future scenarios, Ulva Kvarndamm shows a higher percentage increase in DOC loads than Vattholma.

This comparison shows the difficulties in scaling up catchments, especially if the characteristics differ. Based on the result from the DOC simulations, upscaling Kringlan and Vattholma to represent the entire catchment of Hammarby and Ulva Kvarndamm, both DOC concentrations and loads would have been overestimated. Upscaling should therefore be done with caution and only if the drivers of DOC export in the area are well known. Impacts of catchment size also needs to be considered.

4.5 Implications for drinking water production

DOC loads to both Ekoln and Galten are projected to increase during the coming century under all RCP scenarios. There is a large difference between scenarios and also an important seasonal impact, with a shift towards larger winter loads. It is important to note that the comparison has been made with a reference period 1961-1990, and that previous work has already established that an increase in water colour has occurred since the 1960s in lake Mälaren (Sonesten et al. 2013; Köhler & von Brömssen 2019; Lindqvist 2020).

The DOC loads reaching Galten and Ekoln will be subjected to mineralization, flocculation and photolytic processing as the water is transported towards the outlets in the east of the lake. This means that the increase in DOC loads that are seen in future scenarios to the Galten and Ekoln basins will be dampened in the eastern basins that serve as drinking water sources for Stockholm. Water colour has been shown to be significantly correlated between Galten and Görväln as well as Ekoln and Görväln, where the raw water intake of Norrvatten is located (Lindqvist 2020). The correlation is stronger between Ekoln and Görväln as these have a direct water exchange whereas water from Galten passes two other basins with retention times of 0.6 and 1.8 years before reaching Görväln (Wallin et al. 2000). Increased DOC loads would likely have an effect on the water in the Görväln basin as well, with estimated 30% of the water coming from Ekoln and 70% from the basin Prästfjärden that lies between Galten and Görväln (Köhler & von Brömssen 2019). The faster exchange between Ekoln and Görväln could likely result in a larger impact of seasonal DOC loadings. Higher flows into Galten and Ekoln from surrounding catchments could also result in a shorter lake water retention time, leading to occasionally stronger responses to DOC peaks seen in Görväln, for example during winter storms. Higher DOC concentrations in the Görväln basin would mean that the drinking water treatment plants in Stockholm must adjust the treatment process so that the organic content can be safely removed.

5 Conclusion

The study examined the performance of the GWLF-Hydrology-DOC model in 13 catchments in lake Mälaren, how simulated DOC from these catchments would respond to climate change scenarios RCP2.6, 6.0 and 8.5, and if this could potentially demand more treatment of the lake water in the future to produce acceptable drinking water to the Stockholm area.

The GWLF-Hydrology-DOC model could successfully simulate streamflow and DOC loads from all study catchments. Simulated DOC concentrations were less successful but show good potential. The future climate scenarios showed increased DOC concentration and loads in all catchments and over all RCP scenarios, with largest increase seen under RCP8.5 and lowest under RCP2.6. The increases are strongly impacted by large seasonal changes in streamflow, with a shift towards higher winter DOC concentrations and loads. Both Galten and Ekoln will receive higher winter DOC loads in the future, also resulting in an increased colour in the eastern lake basins which serves as drinking water source to drinking water treatment plant Norrvatten and Stockholm County.

Going forward, the GWLF-DOC model shows much promise in predicting DOC concentrations and loads to lake Mälaren. The easily adaptable interface provided by Vensim allows for modification of the model structure and additional processes can be added as the DOC dynamics in the Mälaren catchments are better understood. To estimate the DOC export to lake Mälaren and its effects on drinking water production, further work also needs to be done on in-lake transport and processes.

6 Acknowledgements

I would like to thank everyone involved in the project. First, thank you to my supervisor Don Pierson at Uppsala University for all your help throughout my thesis and for teaching me all about GWLF and Vensim. Also, thank you to Ricardo Marroquìn Paiz and Eleanor Jennings at the Dundalk Institute of Technology for all the helpful discussions and shared knowledge. Our GWLF modelling meetings and your support were essential to reach this point.

Thank you to Norrvatten for helping me find a thesis subject and to Stephan Köhler, my supervisor at Norrvatten, for advice and encouragement throughout the process. Lastly, thank you to my opponent Rasmus Herløv Jørgenssen and subject reviewer Benjamin Fischer for valuable feedback on my report.

7 References

Aitkenhead-Peterson J.A., McDowell W.H. & Neff J.C. (2003). Sources, production and regulation of allochthonous dissolved organic matter inputs to surface waters. In: Findlay S.E.G. & Sinsabaugh R.L. (eds). *Aquatic ecosystems: interactivity of dissolved organic matter*. 1st edition, Academic Press. 71-91. https://doi.org/10.1016/B978-012256371-3/50003-2

Allen, R.G., Pereira, L.S., Raes, D. and Smith, M., 1998. Crop evapotranspiration-Guidelines for computing crop water requirements-FAO Irrigation and drainage paper 56. *Fao, Rome*, *300*(9), p.D05109.

Arnold, J.G., P.M. Allen, R. Muttiah, and G. Bernhardt. (1995). Automated base flow separation and recession analysis techniques. *Groundwater.* 33(6), 1010-1018. https://doi.org/10.1111/j.1745-6584.1995.tb00046.x

Bosen, J.F. (1960) A FORMULA FOR APPROXIMATION OF THE SATURATION VAPOR PRESSURE OVER WATER. *Monthly Weather Review*. 88, 275-276

Creed, I.F., Bergström, A.K., Trick, C.G. et al. (2018). Global change-driven effects on dissolved organic matter composition: Implications for food webs of northern lakes. *Global Change Biology*. 24 (8), 3692-3714. https://doi.org/10.1111/gcb.14129

Davidson, E. & Janssens, I. (2006). Temperature sensitivity of soil carbon decomposition and feedbacks to climate change. *Nature*. 440**,** 165–173. https://doi.org/10.1038/nature04514

de Wit, H.A., Valinia, S., Weyhenmeyer, G.A., Futter, M.N., Kortelainen, P., Austenes, K., Hessen, D.O., Räike, A., Laudon, H. & Vuorenmaa, J. (2016). Current Browning of Surface Waters Will Be Further Promoted by Wetter Climate. *Environmental Science and Technology Letters* 3: 430–435. https://doi.org/10.1021/acs.estlett.6b00396

Einola, E. (2013). *Present and future fluxes of nitrogen, phosphorus and carbon from catchments to lakes in a boreal landscape*. University of Helsinki. Lahti. ISBN: 978-952-10-8661-8

Eklund, A., Stensen, K., Alavi, G. & Jacobsson, K. (2018). *Sveriges stora sjöar idag och i framtiden*. Rapport / SMHI. Klimatologi nr 49

Finstad, A., Andersen, T., Larsen, S. et al. (2016) From greening to browning: Catchment vegetation development and reduced S-deposition promote organic carbon load on decadal time scales in Nordic lakes. *Sci Rep.* 6, 31944. https://doi.org/10.1038/srep31944

Fischer, B., Seibert, J. & Bishop, K. (2021). Hydrological connectivity effects of forest management interventions measured with isotope hydrograph separation after clear cuts and wetland restoration. *AGU Fall meeting* December 13, 2021, New Orleans, Louisiana, USA. https://agu.confex.com/agu/fm21/meetingapp.cgi/Paper/811221 [2022-05-05]

Fork, M. L., Sponseller, R. A., & Laudon, H. (2020). Changing source-transport dynamics drive differential browning trends in a boreal stream network. *Water Resources Research*. 56(2). https://doi.org/10.1029/2019WR026336

Frieler, K., Lange, S., Piontek, F., Reyer, C., Schewe, J., Warszawski, L., Zhao, F., Chini, L., Denvil, S., Emanuel, K., Geiger, T., Halladay, K., Hurtt, G., Mengel, M., Murakami, D., Ostberg, S., Popp, A., Riva, R., Stevanovic, M., Yamagata, Y. (2017). Assessing the impacts of 1.5°C global warming-Simulation protocol of the Inter-Sectoral Impact Model Intercomparison Project (ISIMIP2b). Geoscientific Model Development. https://doi.org/10.5194/gmd-10-4321-2017

Futter, M. N., D. Butterfield, B. J. Cosby, P. J. Dillon, A. J. Wade, & P. G. Whitehead. (2007), Modeling the mechanisms that control in-stream dissolved organic carbon dynamics in upland and forested catchments. *Water Resources Research.* 43(2). https://doi.org/10.1029/2006WR004960

Futter, M., Löfgren S., Köhler, S. Lundin, L., Moldan, F. & Bringmark, L. (2011). Simulating Dissolved Organic Carbon Dynamics at the Swedish Integrated Monitoring Sites with the Integrated

Catchments Model for Carbon, INCA-C. *Ambio.* 40(8), 906–19. https://doi.org/10.1007/s13280-011-0203-z

Haith, D.A., Mandel, R. & Wu, R.S. (1996). Generalized Watershed Loading Functions: Version 2.0 User's Manual. Cornell University, Department of Agricultural & Biological Engineering, Ithaca, NY.

Haith, D.A. & Shoemaker, L.L. (1987). GENERALIZED WATERSHED LOADING FUNCTIONS FOR STREAM FLOW NUTRIENTS. *Water Resources Bulletin.* 23(3), 471-478. https://doi.org/10.1111/j.1752-1688.1987.tb00825.x

Hamon, W.R. (1961). Estimating Potential Evapotranspiration. Journal of the Hydraulics Division, Proceedings of the American Society of Civil Engineers. 87, 107-120.

Hattermann, F.F., Vetter, T., Breuer, L., Buda, S., Daggupati, P., Donnelly, C., Fekete, B., Flörke, F., Gosling, S.N., Hoffmann, P., Liersch, S., Masaki, Y., Motovilov, Y., Müller, C., Samaniego, L., Stacke, T., Wada, Y., Yang T. & Krysnaova, V. (2018). Sources of uncertainty in hydrological climate impact assessment: a cross-scale study. *Environmental Research Letters.* 13(1) 015006. https://doi.org/10.1088/1748-9326/aa9938

Haylock, M. R., Hofstra, N., Tank, A., Klok, E. J., Jones, P. D., & New, M. (2008). A European daily high-resolution gridded data set of surface temperature and precipitation for 1950–2006. Journal of Geophysical Research-Atmospheres, 113. D20119, doi: https://doi.org/10.1029/2008jd010201

IPCC, 2014: *Climate Change 2014: Synthesis Report. Contribution of Working Groups I, II and III to the Fifth Assessment Report of the Intergovernmental Panel on Climate Change* [Core Writing Team, R.K. Pachauri and L.A. Meyer (eds.)]. IPCC, Geneva, Switzerland, 151 pp

Jennings, E., Allott, N., Pierson, D.C., Schneiderman, E.M., Lenihan, D., Samuelsson, P. & Taylor, D. (2009). Impacts of climate change on phosphorus loading from a grassland catchment: implications for future management. *Water Research*. 43(17), 4316-26. https://doi.org/10.1016/j.watres.2009.06.032

Jungqvist, G., Oni, S., Teutschbein, C., & Futter, M. (2014). Effect of Climate Change on Soil Temperature in Swedish Boreal Forests. *PloS one*. 9(4) e93957. https://doi.org/10.1371/journal.pone.0093957

Karhu, K., Fritze, H., Tuomi, M., Vanhala, P., Spetz, P., Kitunen, V. & Liski, J. (2010). Temperature sensitivity of organic matter decomposition in two boreal forest soil profiles. *Soil Biology and Biochemistry*. 42 (1), 72-82. https://doi.org/10.1016/j.soilbio.2009.10.002

Klimek, B., Chodak, M., Jaźwa, M., Azarbad, H., & Niklińska, M. (2020). Soil physicochemical and microbial drivers of temperature sensitivity of soil organic matter decomposition under boreal forests. *Pedosphere*. 30 (4), 528-534. https://doi.org/10.1016/S1002-0160(17)60400-4

Kritzberg, E. S. & Ekström, S. M. (2012). Increasing iron concentrations in surface waters-a factor behind brownification? *Biogeosciences.* 9, 1465–1478. https://doi.org/10.5194/bg-9-1465-2012

Kritzberg, E.S., Hasselquist, E.M., Škerlap, M., Löfgren S., Olsson, O., Stadmark, J., Valinia, S., Hansson, L-A. & Laudon, H. (2020). Browning of freshwaters: Consequences to ecosystem services, underlying drivers, and potential mitigation measures. *Ambio* 49: 375–390. https://doi.org/10.1007/s13280-019-01227-5

Köhler, S.J., Kothawala, D., Futter, M.N., Ljungman, O.L. & Tranvik, L. (2013). In-Lake Processes Offset Increased Terrestrial Inputs of Dissolved Organic Carbon and Colour to Lakes. PLoS ONE 8 (8): e70598. https://doi.org/10.1371/journal.pone.0070598

Köhler, S.J., Lavonen, E. Keucken, A., Schmitt-Kopplin, P. Spanjer, T. & Persson, K. (2016). Upgrading coagulation with hollow-fibre nanofiltration for improved organic matter removal during surface water treatment. *Water Research.* 89, 232-240. https://doi.org/10.1016/j.watres.2015.11.048

Köhler, S. & von Brömssen, C., (2021). *Sammanställning av långsiktiga vattenkemiska förändringar i Mälaren och övergripande analys av möjliga drivvariabler och trender.* (2021:5). Uppsala: Institutionen för vatten och miljö, Sveriges lantbruksuniversitet. http://urn.kb.se/resolve?urn=urn:nbn:se:slu:epsilon-p-110882

Lapierre, J.F., Guillemette, F., Berggren, M. & del Giorgio, P.A. (2013). Increases in terrestrially derived carbon stimulate organic carbon processing and CO_2 emissions in boreal aquatic ecosystems. *Nature Communications.* 4, 2972. https://doi.org/10.1038/ncomms3972

Lavonen, E.E., Gonsior, M., Tranvik, L.J., Schmitt-Kopplin, P. & Köhler, S. (2013). Selective Chlorination of Natural Organic Matter: Identification of Previously Unknown Disinfection Byproducts. *Sci. Technol.* 47 (5), 2264–2271. https://doi.org/10.1021/es304669p

Ledesma, J.L.J., Köhler, S.J. & Futter, M. N. (2012). Long-term dynamics of dissolved organic carbon: Implications for drinking water supply. *Science of The Total Environment.* 432, 1-11. https://doi.org/10.1016/j.scitotenv.2012.05.071

Ledesma, J. L. J., Kothawala, D. N., Bastviken, P., Maehder, S., Grabs, T., & Futter, M. N. (2018). Stream dissolved organic matter composition reflects the riparian zone, not upslope soils in boreal forest headwaters. *Water Resources Research*. 54, 3896–3912. https://doi.org/10.1029/2017WR021793

Lindqvist, Klara (2020). *Brownification of lake Mälaren: Effects of land use and climate change.* Umeå University. Department of Ecology and Environmental Science/Earth Science. diva2:1439142

Mitchell, G.N., & McDonald, A.T. (1992). Discolouration of water by peat following induced drought and rainfall simulation. *Water Research.* 26(3), 321-326. https://doi.org/10.1016/0043-1354(92)90029-4

Monteith, D. T., Stoddard, J. L., Evans, C. D., de Wit, H. A., Forsius, M., Høgåsen, T., Wilander, A., Skjelkvåle, B. L., Jeffries, D. S., Vuorenmaa, J., Keller, B., Kopácek, J. och Vesely, J. (2007). Dissolved organic carbon trends resulting from changes in atmospheric deposition chemistry. *Nature* 450: 537–540. https://doi.org/10.1038/nature06316

Moore, K. (2007). *Climate Change Impacts on the Catchment Contribution to Lake Water Quantity and Quality*. Diss. Uppsala University. Uppsala. http://urn.kb.se/resolve?urn=urn:nbn:se:uu:diva-8236

Moore, K., Pierson, D., Pettersson, K., Schneiderman, E. & Samuelsson, P. (2008). Effects of warmer world scenarios on hydrologic inputs to Lake Mälaren, Sweden and implications for nutrient loads. *Hydrobiologica*. 599, 191–199. https://doi.org/10.1007/s10750-007-9197-8

Naden, P., Allott, N., Arvola, L., Järvinen, M., Jennings, E., Moore, K., Aonghusa, C., Pierson, D. & Schneiderman, E. (2009). Modelling the Impacts of Climate Change on Dissolved Organic Carbon. *The Impact of Climate Change on European Lakes*. 221-252. https://doi.org/10.1007/978-90-481-2945-4_13

Nash, J.E. & Sutcliffe, J.V. (1970). River flow forecasting through conceptual models, part I—A discussion of principles. *Journal of Hydrology*. 10, 282-290. https://doi.org/10.1016/0022-1694(70)90255-6

Niraula, R., Kalin, L., Srivastava, P. & Anderson, C.J. (2013). Identifying critical source areas of nonpoint source pollution with SWAT and GWLF. *Ecological Modelling*. 268, 123-133. https://doi.org/10.1016/j.ecolmodel.2013.08.007

Norrvatten. (n.d.). *Dricksvattenproduktion.* https://www.norrvatten.se/dricksvatten/dricksvattenproduktion/ [2022-01-25]

Oni, S.K., Futter, M.N., Moldot, L.A. & Dillon, P.J., (2012). Modelling the long term impact of climate change on the carbon budget of Lake Simcoe, Ontario using INCA-C. *Science of the Total Environment.* 414, 387-403. https://doi.org/10.1016/j.scitotenv.2011.10.025

Qi, Z., Gelin, K., Chunli, C., Yu, Q., Ze, X. & Yuqiu, W. (2017). Comparison of SWAT and GWLF Model Simulation Performance in Humid South and Semi-Arid North of China. *Water*. 9(8), 567. https://doi.org/10.3390/w9080567

Richardson, S.D., Plewa, M.J., Wagner, E.D., Schoeney, R. & DeMarini, D.M. (2007). Occurrence, genotoxicity, and carcinogenicity of regulated and emerging disinfection by-products in drinking

water: A review and roadmap for research. *Mutation Research* 636: 178–242. https://doi.org/10.1016/j.mrrev.2007.09.001

Seibert, J. (1999). Regionalisation of parameters for a conceptual rainfall-runoff model. *Agricultural and Forest Meteorology*. 98-99, 279-293. https://doi.org/10.1016/S0168-1923(99)00105-7

Schneiderman, E.M., Pierson, D., Lounsbury, D.G. & Zion M.S. (2002). Modeling the hydrochemistry of the cannonsville watershedwith generalized watershed loading functions (GWLF). *Journal of the American Water Resources Association*. 38(5), 1323-1347. https://doi.org/10.1111/j.1752-1688.2002.tb04350.x

Schneiderman, E.M., Järvinen, M., Jennings, E., May, L., Moore, K.E., Naden, P.S., & Pierson, D.C. (2009). Modeling the Effects of Climate Change on Catchment Hydrology with the GWLF Model. *The Impact of Climate Change on European Lakes*. 33-50. https://doi.org/10.1007/978-90-481-2945-4_3

Škerlep, M., Steiner, E., Axelsson, A-L. & Kritzberg, E.S. (2019). Afforestation driving long-term surface water browning. *Global Change Biology* 00: 1-10. https://doi.org/10.1111/gcb.14891

SLU. (2022). *Vattenfärg-absorbans.* https://www.slu.se/institutioner/vatten-miljo/laboratorier/vattenkemiska-laboratoriet/detaljerade-metodbeskrivningar/absorbans/ [2022-03-15]

Sonesten, L., Wallman, K., Axenrot, T., Beier, U., Drakare, S., Ecke, F., Goedkoop, W., Grandin, U., Köhler, S., Segersten, J. & Vrede, T. (2013). *Mälaren Tillståndsutvecklingen 1965–2011*. Rapport/ Sveriges lantbruksuniversitet 2013:1. Uppsala.

Stockholm vatten och avfall. (n.d.). *Vattenverk.* https://www.stockholmvattenochavfall.se/om-oss/projekt-och-samrad/stadsovergripande-projekt/vi-sakrar-stockholms-vattenforsorjning/vattenverk/ [2022-01-25]

Temnerud, J. (2005). *Spatial Variation of Dissolved Organic Carbon along Streams in Swedish Boreal Catchments.* Diss. Örebro University. Örebro University: University Library. ISBN: *91-7668-437-7*

Vanhala, P., Karhu, K., Tuomi, M., Björklöf, K., Fritze, H. & Liski, J. (2008). Temperature sensitivity of soil organic matter decomposition in southern and northern areas of the boreal forest zone. *Soil Biology and Biochemistry*. 40(7), 1758-1764. https://doi.org/10.1016/j.soilbio.2008.02.021

von Arnold, K., Weslien, P., Nilsson, M., Svensson, B.H. & Klemedtsson, L. (2005). Fluxes of CO2, CH4 and N2O from drained coniferous forests on organic soils. *Forest Ecology and Management.* 210(1–3), 239-254. https://doi.org/10.1016/j.foreco.2005.02.031

von Wachenfeldt E. & Tranvik L.J. (2008). Sedimentation in boreal lakes-The role of flocculation of allochthonous dissolved organic matter in the water column. *Ecosystems.* 11, 803-814. https://doi.org/10.1007/s10021-008-9162-z

Wallin, M., Andersson, B., Johnson, R., Kvarnäs, H., Persson, G., Weyhenmeyer, G. & Willén, E. (2000). *Mälaren-miljötillstånd och utveckling 1965–98*. Rapport/ Mälarens vattenvårdsförbund. Västerås: Länsstyrelsen Västmanlands län.

Wickland, K. & Neff, J. (2007). Decomposition of soil organic matter from boreal black spruce forest: environmental and chemical controls. *Biogeochemistry.* 87(1): 29-47. https://doi.org/10.1007/s10533-007-9166-3

Appendix 1: Hydrology validation

Hydrology validation graphs for the 10-year periods used for each catchment, except for Fellingsbro and Vattholma that are included in the report. Graphs are showing measured and simulated streamflow, baseflow and runoff for every catchment.

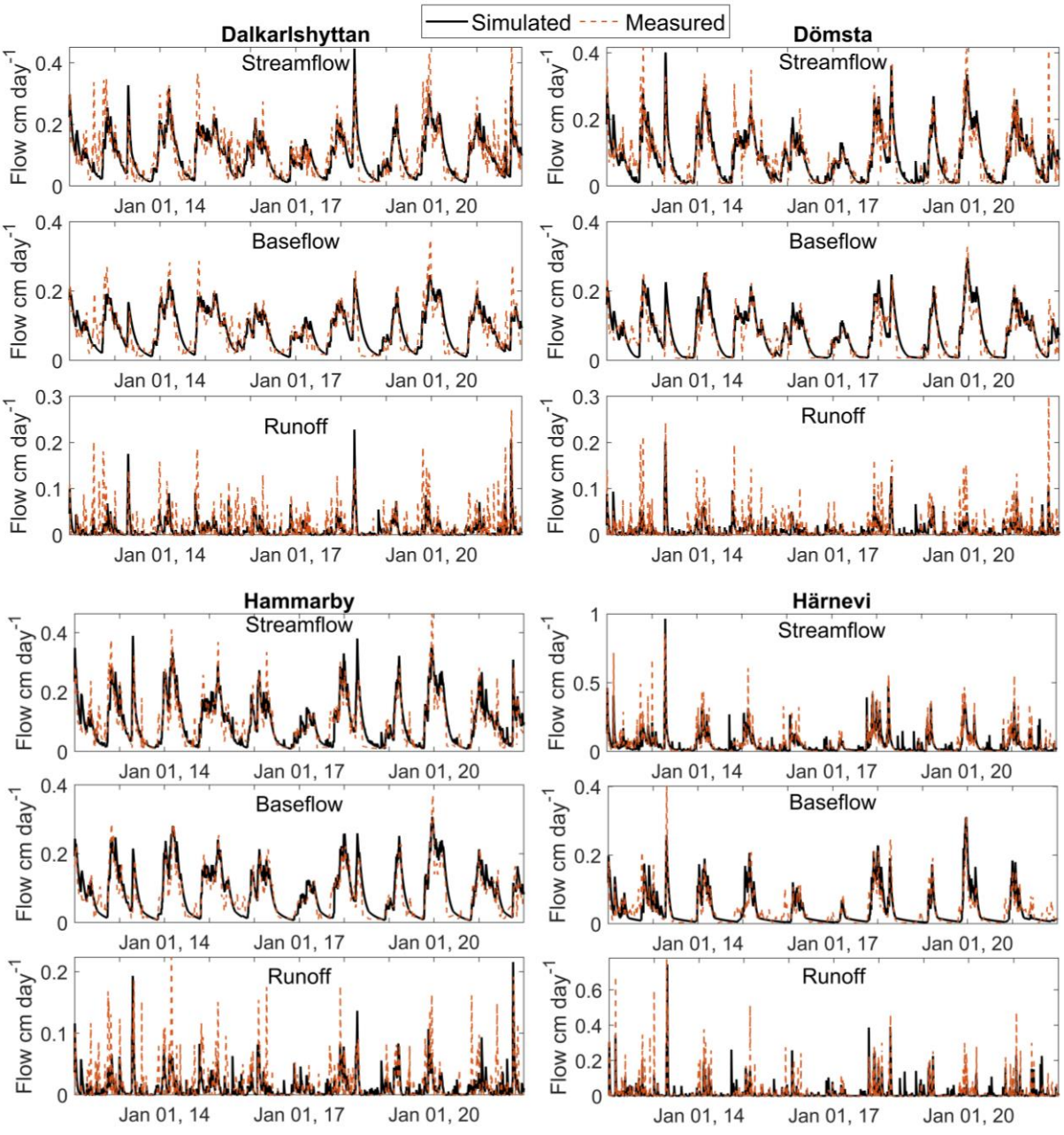

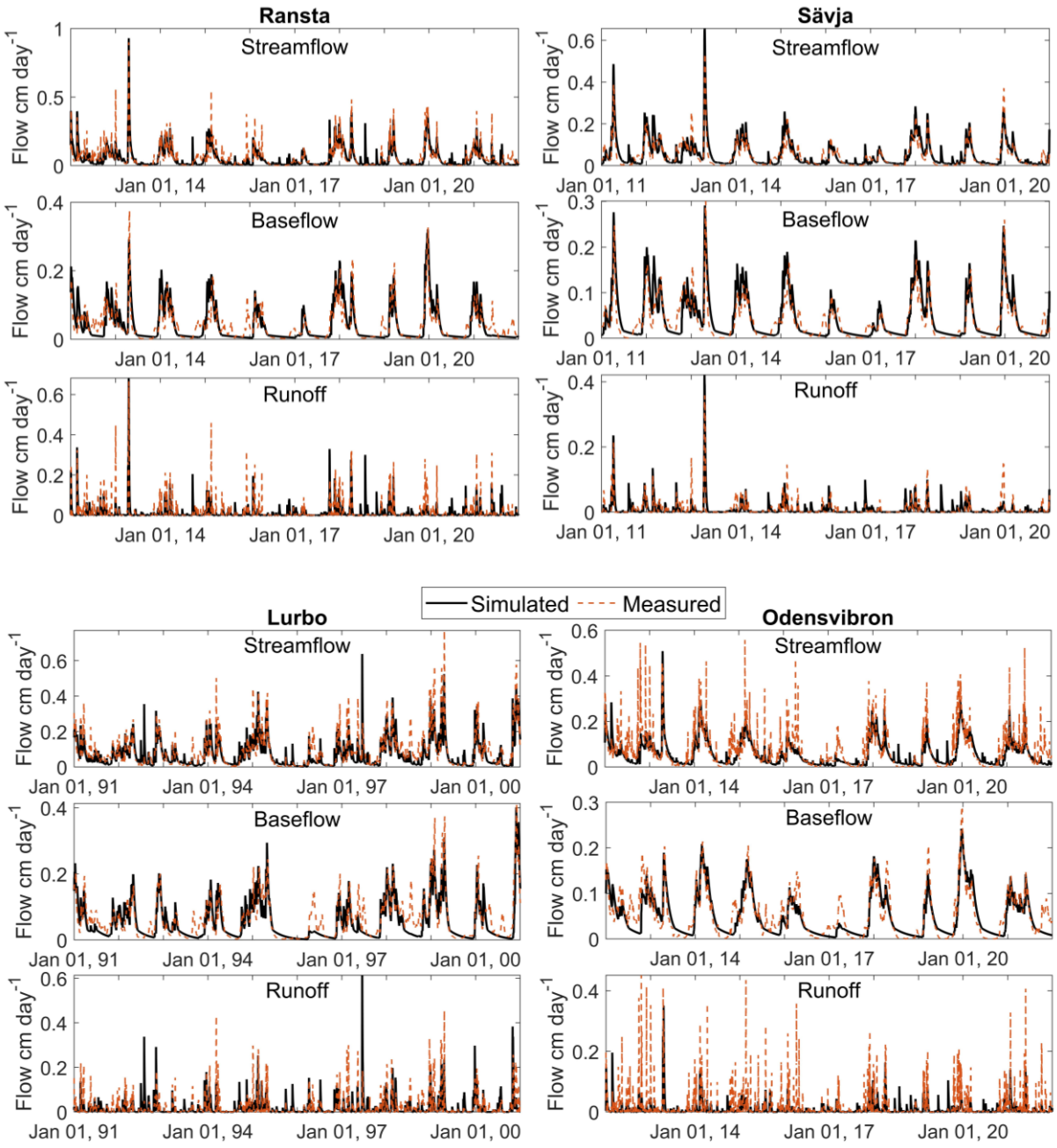
Ransta
Sävja
Lurbo
Odensvibron
Streamflow
Baseflow
Runoff
Simulated
Measured
Flow cm day-1
Jan 01, 11
Jan 01, 14
Jan 01, 17
Jan 01, 20
Jan 01, 91
Jan 01, 94
Jan 01, 97
Jan 01, 00

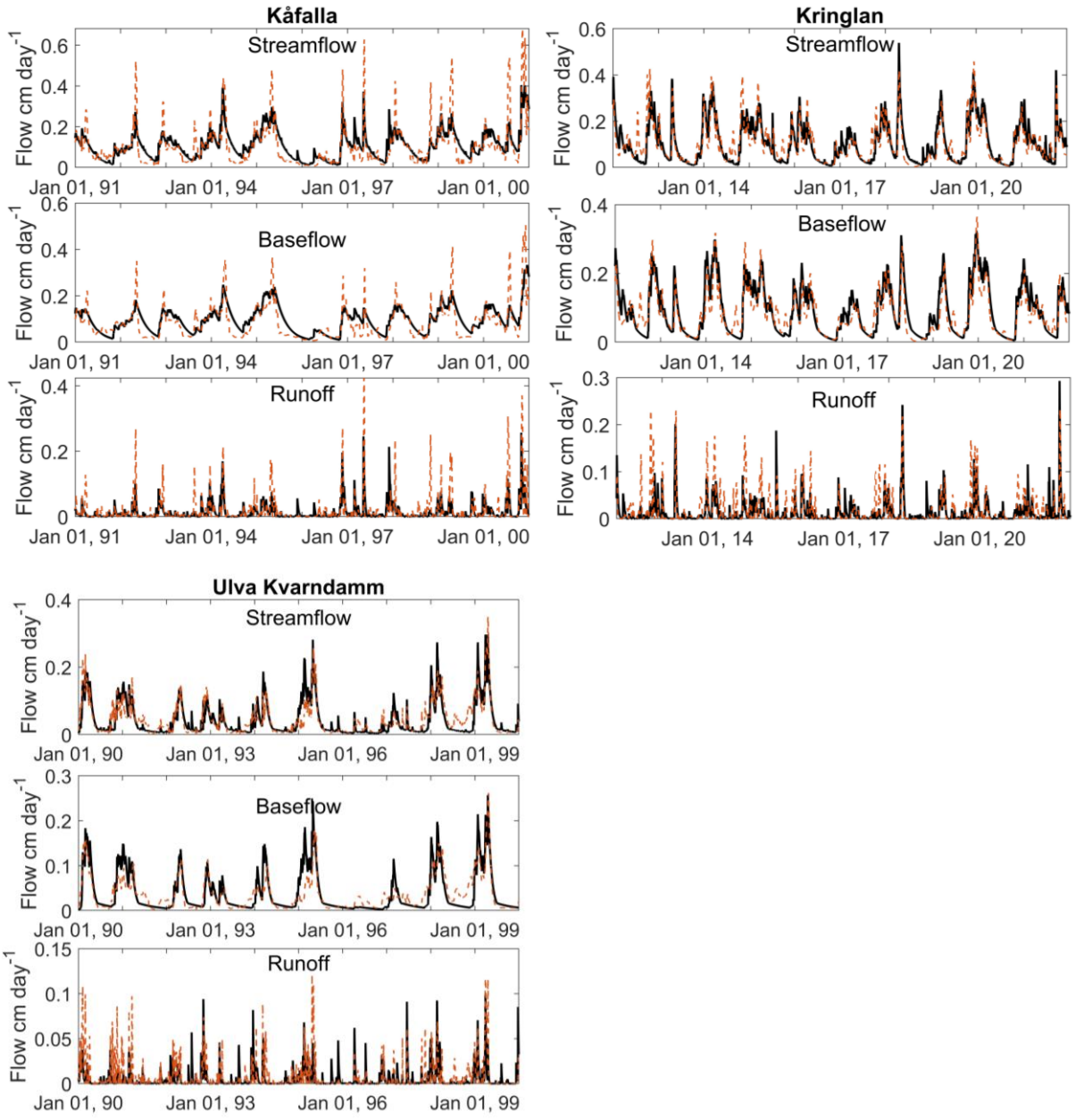
Kåfalla
Streamflow
Baseflow
Runoff
Kringlan
Streamflow
Baseflow
Runoff
Ulva Kvarndamm
Streamflow
Baseflow
Runoff
Flow cm day-1
Jan 01, 91
Jan 01, 94
Jan 01, 97
Jan 01, 00
Jan 01, 14
Jan 01, 17
Jan 01, 20
Jan 01, 90
Jan 01, 93
Jan 01, 96
Jan 01, 99

Appendix 2: DOC calibration

DOC calibration graphs for all catchments but Fellingsbro and Vattholma, that are already presented in the report. First, graphs with measured DOC concentrations, simulated DOC concentrations and simulated streamflow are shown for each catchment. After these, graphs showing daily and monthly DOC loads, based on measured streamflow and interpolated DOC measurements as well as simulated DOC concentrations and streamflow.

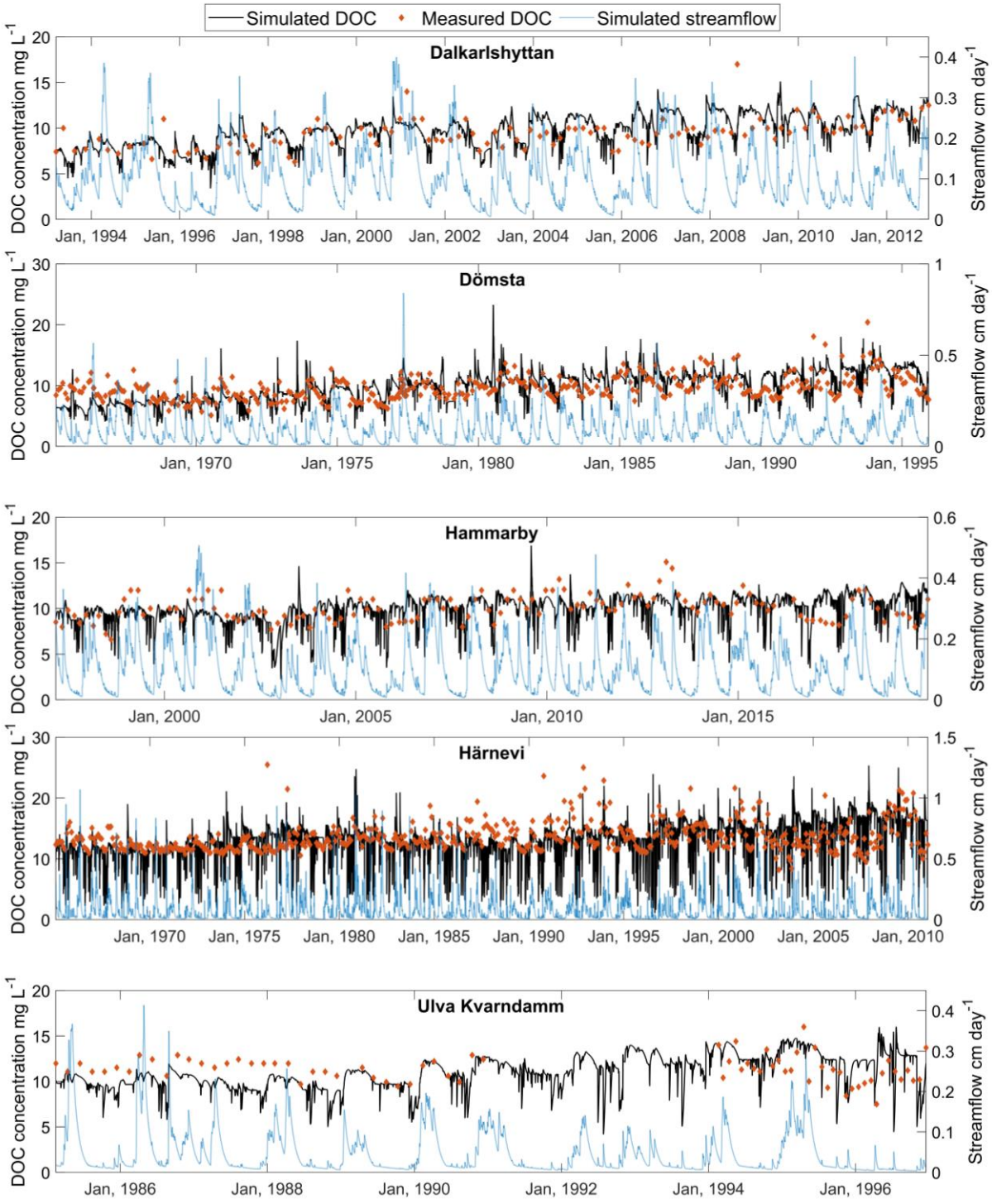

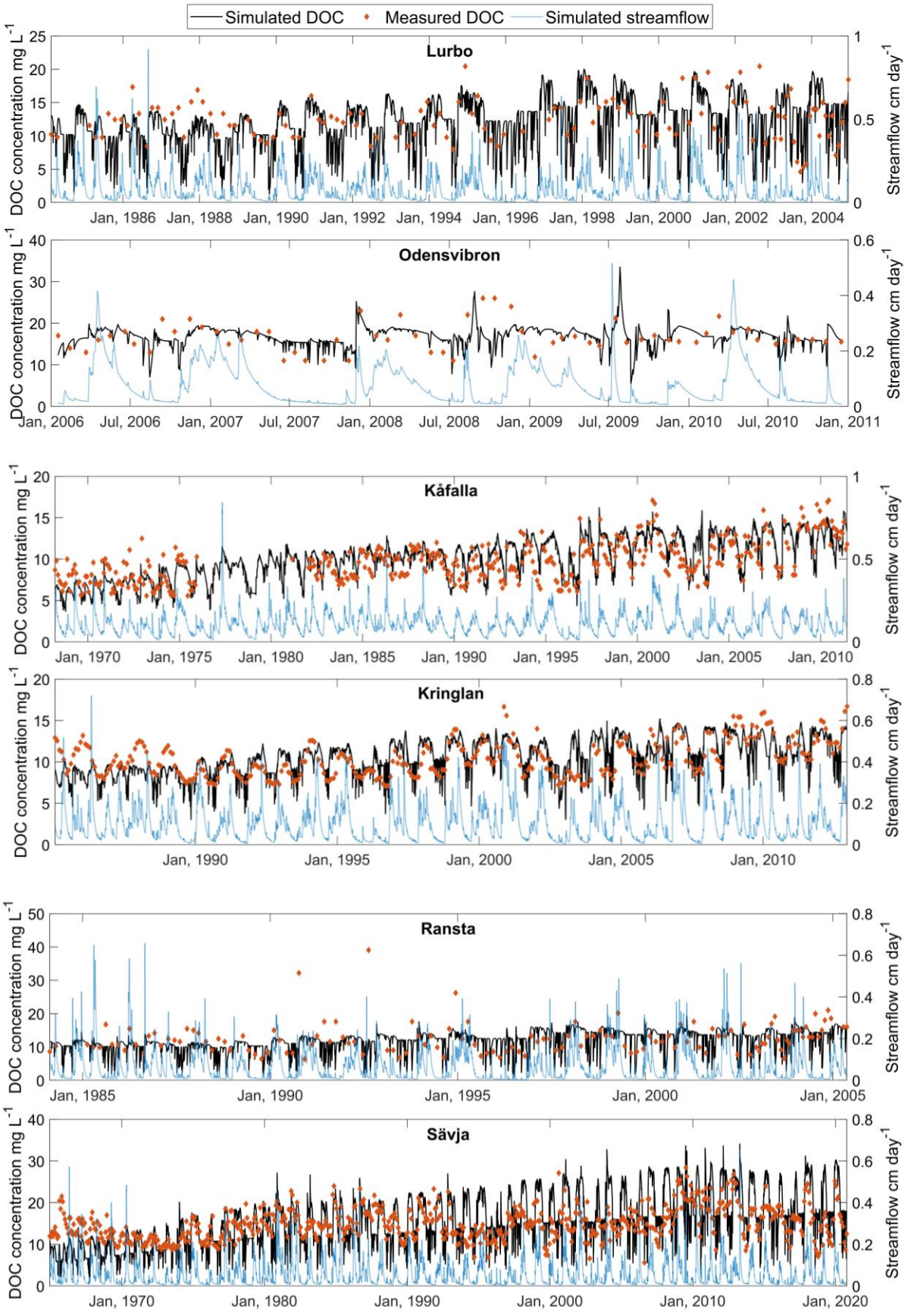
Simulated DOC
Measured DOC
Simulated streamflow
Lurbo
Odensvibron
Kåfalla
Kringlan
Ransta
Sävja
DOC concentration mg L-1
Streamflow cm day-1

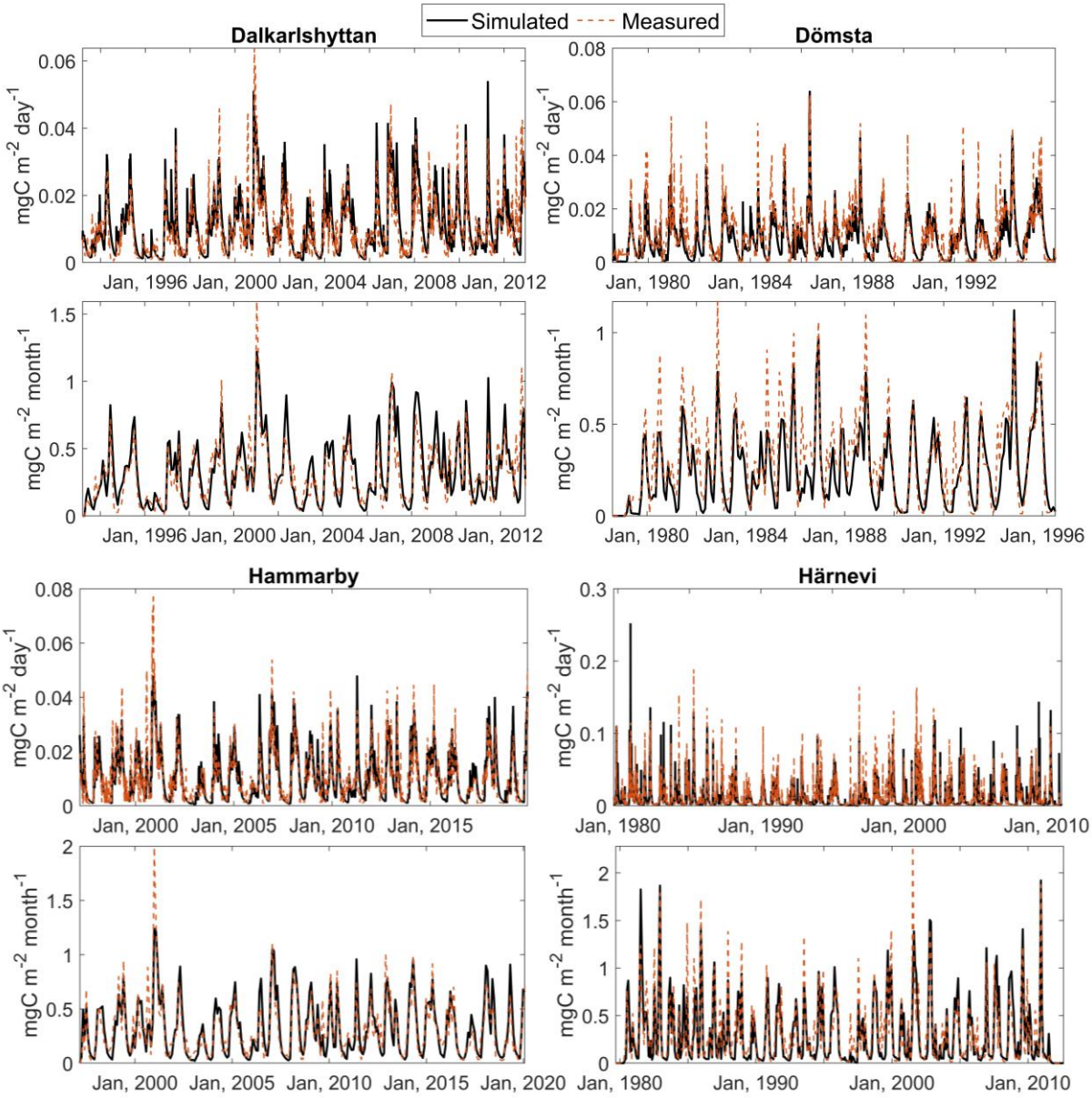
Simulated
Measured
Dalkarlshyttan
Dömsta
Hammarby
Härnevi
mgC m-2 day-1
mgC m-2 month-1
Jan, 1996 Jan, 2000 Jan, 2004 Jan, 2008 Jan, 2012
Jan, 1980 Jan, 1984 Jan, 1988 Jan, 1992
Jan, 1996 Jan, 2000 Jan, 2004 Jan, 2008 Jan, 2012
Jan, 1980 Jan, 1984 Jan, 1988 Jan, 1992 Jan, 1996
Jan, 2000 Jan, 2005 Jan, 2010 Jan, 2015
Jan, 1980 Jan, 1990 Jan, 2000 Jan, 2010
Jan, 2000 Jan, 2005 Jan, 2010 Jan, 2015 Jan, 2020
Jan, 1980 Jan, 1990 Jan, 2000 Jan, 2010

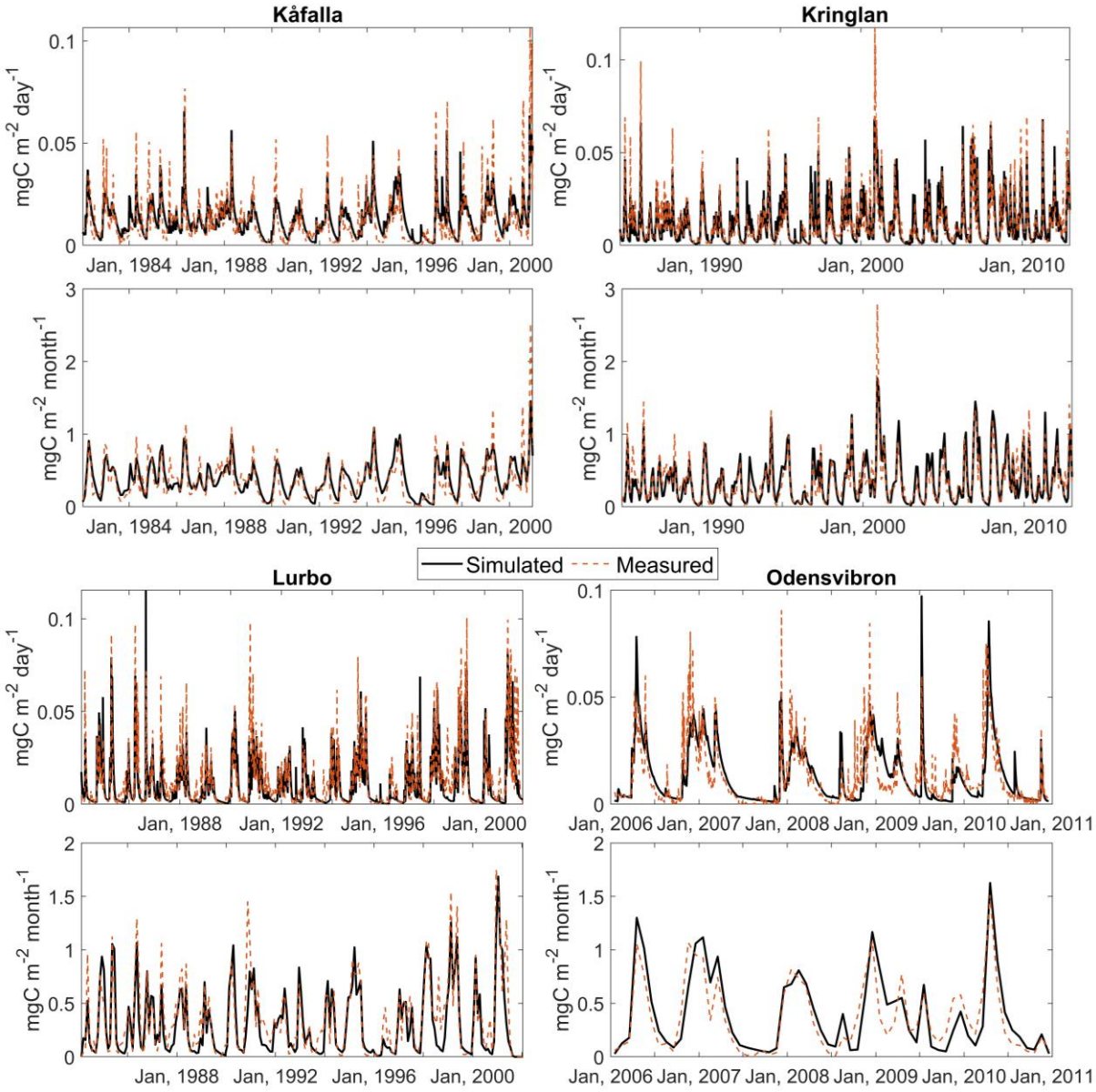
Kåfalla
Kringlan
Lurbo
Odensvibron
Simulated
Measured
mgC m-2 day-1
mgC m-2 month-1
Jan, 1984
Jan, 1988
Jan, 1992
Jan, 1996
Jan, 2000
Jan, 1990
Jan, 2000
Jan, 2010
Jan, 2006
Jan, 2007
Jan, 2008
Jan, 2009
Jan, 2010
Jan, 2011

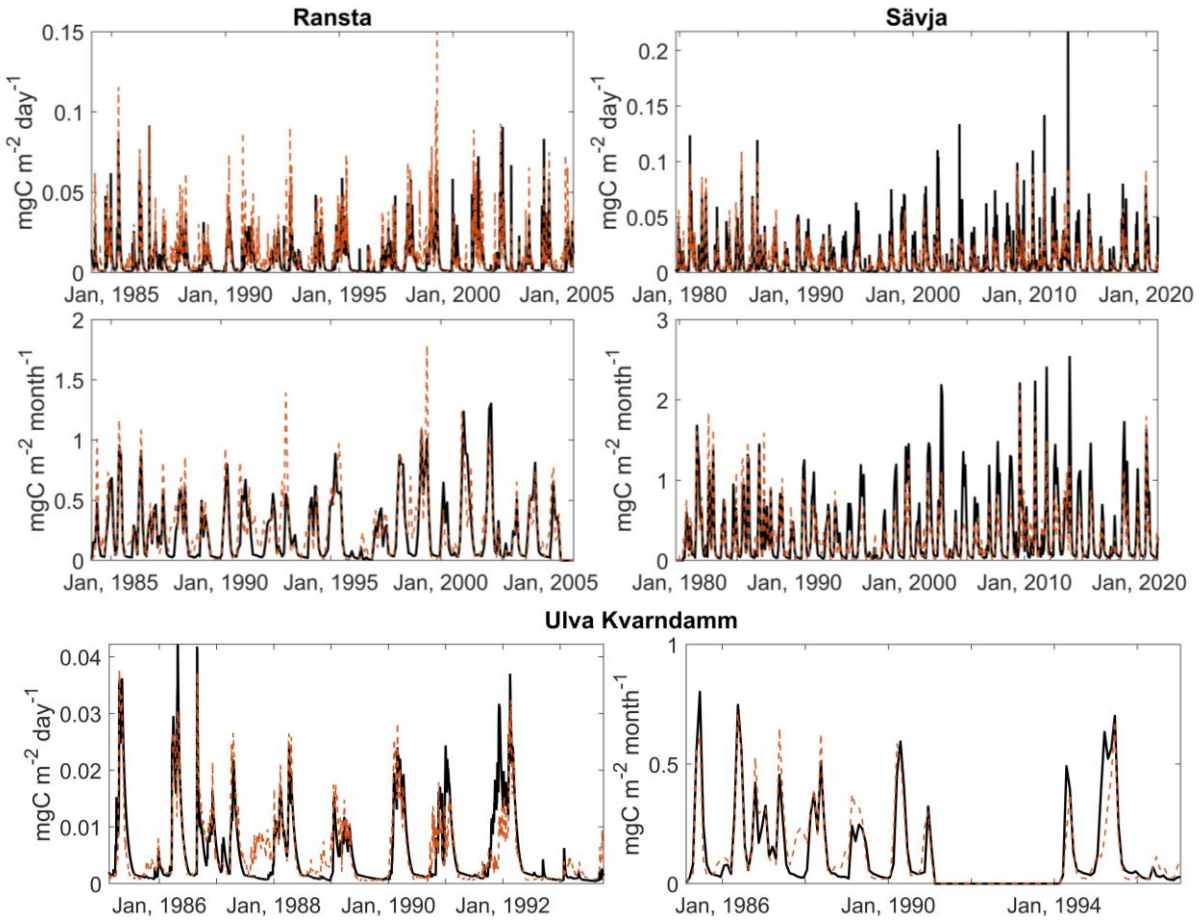
Ransta
Sävja
mgC m-2 day-1
mgC m-2 month-1
Jan, 1985
Jan, 1990
Jan, 1995
Jan, 2000
Jan, 2005
Jan, 1980
Jan, 2010
Jan, 2020
Ulva Kvarndamm
Jan, 1986
Jan, 1988
Jan, 1992
Jan, 1994

Examensarbete vid Institutionen för geovetenskaper
ISSN 1650-6553